Advanced Fiber Materials (2022) 4:1434–1462
https://doi.org/10.1007/s42765-022-00202-2

REVIEW

Electrospun Fibrous Sponges: Principle, Fabrication, and Applications

Dingding Zong[1] · Xinxin Zhang[2] · Xia Yin[2] · Fei Wang[2] · Jianyong Yu[2] · Shichao Zhang[2] · Bin Ding[1,2]

Received: 22 June 2022 / Accepted: 25 August 2022 / Published online: 4 October 2022

Abstract

Electrospun nanofiber materials, with the advantages of large specific surface area, small pore size, high porosity, good channel connectivity, and ease of functional modification, have been widely used in various fields including environmental governance, safety protection, and tissue engineering. With the development of functional fiber materials, the construction of three-dimensional (3D) fiber materials with stable structures has become a critical challenge to expanding application and improving the performance of electrospun fibers. In recent years, researchers have carried out a lot of studies on the 3D reconstruction of electrospun fiber membranes and direct electrospinning of fiber sponges. Specifically, a variety of 3D fibrous sponges were constructed by the 3D reconstruction of electrospun fiber membranes, including embedded hydrogels, 3D printing, gas-foaming, and freeze-drying methods. Meanwhile, the direct electrospinning methods of 3D fibrous sponges have also been successfully developed, which are mainly divided into layer-by-layer stacking, liquid-assisted collection, 3D template collection, particle leaching, and humidity field regulation. Moreover, the applications of these fibrous sponges in many fields have been explored, such as sound absorption, warmth retention, thermal insulation, air filtration, adsorption/separation, and tissue engineering. These research works provide new ideas and methods for the fabrication of 3D fiber materials. Herein, the electrospinning technology and principle were briefly introduced, the representative progress of 3D fiber sponges in recent years was summarized, and their future development prospected.

Keywords Electrospun fibers · Fiber sponges · Preparation · Applications

Introduction

As an important basic and strategic material, fiber not only meets the needs of our daily life, but also is widely used in high-tech fields such as aerospace, environment, and health care [1–4]. In the development process of fiber, fiber refinement is one of the important development trends of fiber materials [5, 6]. When the fiber diameter decreases from micrometers to nanometers, the size effect and surface effect brought by the diameter refinement will endow fiber materials with many unique properties, which can significantly improve the application performance of fiber materials [7–10]. Broadly speaking, fibers with a diameter of less than 1 μm can be called nanofibers, the size effect of nanofibers is very significant, showing many novel characteristics in light, heat, magnetism, electricity, and so on [11–14]. The preparation techniques of nanofibers mainly include the stretching method, template synthesis method, flash-spinning method, islands-in-a-sea method, and electrospinning method [15, 16]. Among them, the technical level of the stretching method and template synthesis method is still in the stage of laboratory research, suffering from narrow raw material range and poor fiber continuity [17]; flash-spinning and islands-in-a-sea methods have high preparation efficiency but suffer from wide fiber diameter distribution or poor controllability of fiber aggregates. Alternatively, electrospinning has become one of the main ways to prepare nanofiber materials because of its abundant raw materials, controllable fiber structure, and good scalability of the preparation process [18, 19].

✉ Shichao Zhang
shichaozhang@dhu.edu.cn

✉ Bin Ding
binding@dhu.edu.cn

[1] State Key Laboratory for Modification of Chemical Fibers and Polymer Materials, College of Materials Science and Engineering, Donghua University, Shanghai 201620, China

[2] Innovation Center for Textile Science and Technology, Donghua University, Shanghai 200051, China

The schematic diagram of the electrospinning process is illustrated in Fig. 1a [20]. The spinning solution or melt is charged and deformed under high-voltage static electricity, and conical droplets are formed at the end of the nozzle [21]. When the charge repulsion on the droplet surface is greater than its surface tension, solution trickles will be ejected from the droplet surface at a high speed. These jets will be stretched by electric field force during short-distance flight and then solidified into fibers along with the volatilization of solvent, finally deposited on the receiving device to form polymer fiber materials [20]. The diameter of the fibers obtained by electrospinning is generally several hundred nanometers, and the electrospun fiber aggregates have the characteristics of small pore size, high porosity, and good fiber continuity, showing broad application prospects in the fields of environmental governance, safety protection, and tissue engineering [22]. However, traditional electrospun fibers are usually assembled into two-dimensional (2D) fiber membranes (thickness of less than 100 μm) with anisotropic structural characteristics, and it is difficult for the fibers to penetrate and interlace effectively in the direction perpendicular to the deposition plane [23, 24]. They suffer from poor resilience and ease of peeling between layers, which greatly affects their practical application in many fields. Compared with 2D electrospun fiber membrane materials, the interlaced and interconnected structures endow 3D fiber materials with good connectivity networks and high specific surface area [25, 26]. On the one hand, the hierarchical micro/nanonetworks of 3D fiber materials can achieve efficient absorption/insulation and selective transport of

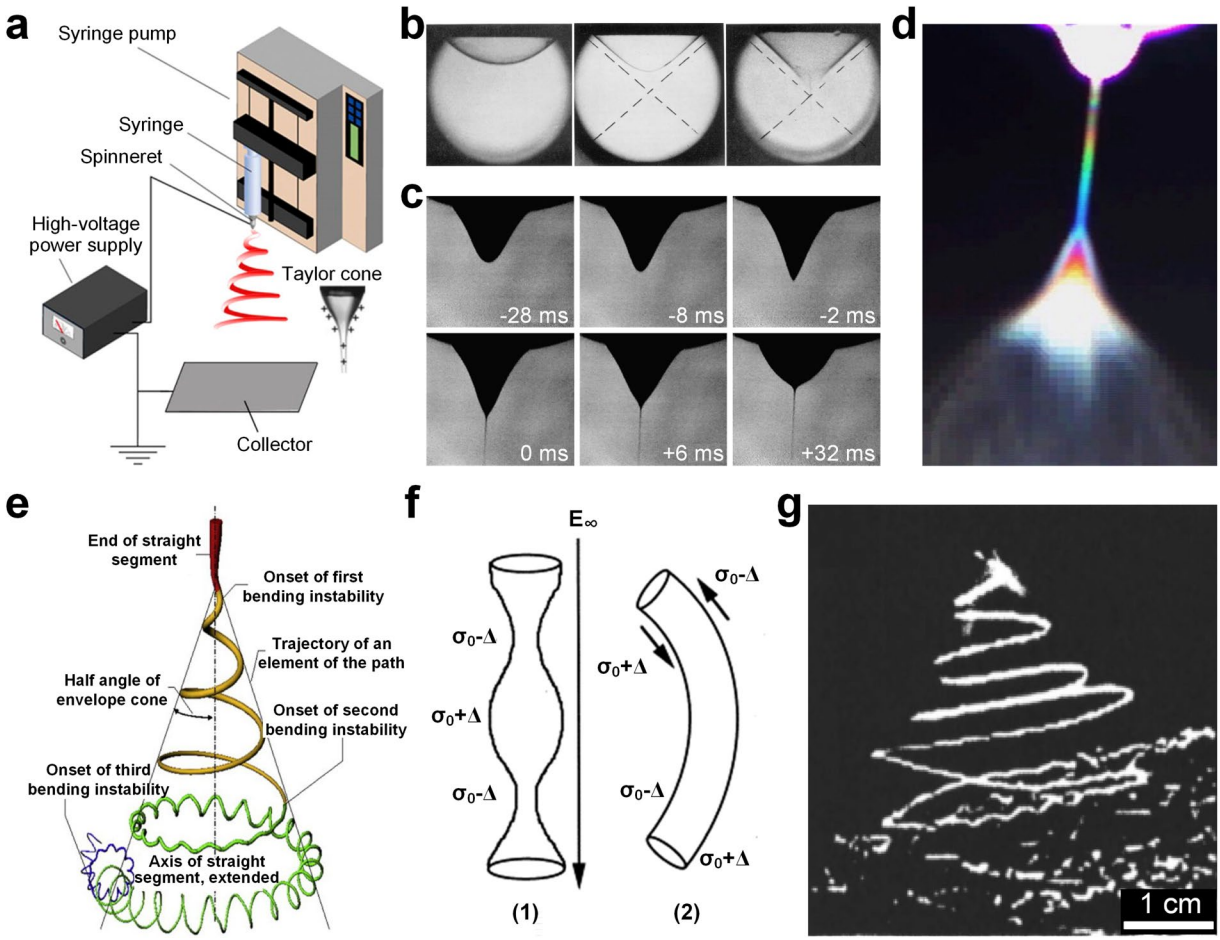

Fig. 1 **a** Schematic diagram of a typical electrospinning device; Reproduced with permission from Ref. [20]; Copyright 2017, American Chemical Society. Taylor cone in 1a; Reproduced with permission from Ref. [36]; Copyright 2004, John Wiley and Sons. **b** The formation process of Taylor cone; Reproduced with permission from Ref. [37]; Copyright 1964, Royal Society of London. **c** The dynamic process of PEO droplet forming jet under electric field; **d** image of the straight section of the jet illuminated by white light; Reproduced with permission from Ref. [38]; Copyright 2008, Elsevier. **e** Schematic diagram of the onset and development of jet instability; Reproduced with permission from Ref. [39]; Copyright 2006, American Chemical Society. **f** Schematic illustration of (1) axisymmetric instability and (2) non-axisymmetric instability of a jet under an electric field; Reproduced with permission from Ref. [40]; Copyright 2001, Elsevier. **g** Stereoscopic image of a jet in the unstable section; Reproduced with permission from Ref. [39]; Copyright 2006, American Chemical Society

continuous media, which can effectively improve the application performance in the fields of sound absorption [27, 28], thermal insulation [29, 30], and adsorption separation [31, 32]. On the other hand, the highly porous structures of 3D fibrous materials have good adaptability to the cell proliferation space, which can effectively simulate the extracellular matrix (ECM) environment of biological tissues, showing great potential in the tissue engineering field [24]. Therefore, the construction of structurally stable 3D fiber materials has become the key challenge to improving the performance of current electrospinning fibers.

Recently, researchers have carried out a lot of studies on two aspects: the 3D reconstruction of electrospun fiber membranes and the direct electrospinning of fiber sponges. They are committed to breaking the inherent layered stacking structure of electrospun fiber materials and building 3D networks with isotropic fiber distribution in the 3D space. Specifically, a variety of 3D nanofibrous sponges were constructed by embedding in hydrogels, 3D printing method, gas-foaming method, and freeze-drying method. Moreover, a series of direct electrospinning methods of fiber sponges have also been successively developed, including layer-by-layer stacking, liquid-assisted collection, 3D template collection, particle leaching, and humidity field regulation. These works provide novel ideas for the construction of 3D fiber sponges. On this basis, the representative progress of 3D fiber materials in recent years was reviewed and an outlook on their future development was given.

Electrospinning Technique

Electrospinning involves the electrohydrodynamic process, in which the polymer solution or melt is charged by the high-voltage electrostatic field and forms a suspended conical droplet at the end of the nozzle [33]. When the charge repulsion force of the droplet surface exceeds its surface tension, the polymer solution trickle will be sprayed at high speed on the droplet surface, which is referred to as a "jet" [34]. These jets will undergo high-speed stretching, solvent volatilization, and solidification in a short distance under electric field force. Finally, they are deposited on the receiving plate to obtain fibers. The electrospun fibers possess a small diameter (generally between a few nanometers and a few micrometers) and a large specific surface area; and the fiber sponges have the advantages of small pore size, high porosity, and good pore connectivity [35].

Principle of Electrospinning

In 1934, Formhals invented the devices for the preparation of polymer nanofibers by electrostatic field force and applied for a patent, which is recognized as the beginning of electrospinning. A typical electrospinning device is mainly composed of a high-voltage power supply, a liquid supply device (including spinning nozzles), and receiving device (Fig. 1a) [20, 36]. The high voltage power supply provides a high voltage for generating spinning jets, and the positive and negative poles of the power supply are connected with the spinning nozzle and the receiving device, respectively [41]. When the jet moves in the air, it is accompanied by solvent volatilization and jet solidification, finally depositing on the receiving device to form a fiber aggregate [42]. There are two main stages from jet ejection to fiber formation: (1) Jets formation and initial motion. The spinning solution jets are pulled out at the spinneret and move along a straight line. (2) Stretching, thinning, and solidification of jets. After a short distance of stable stretching, the jet would occur unstable whiplash, further stretch and refine, and then solidify and deposited into fibers [43].

Electrospinning is a special case of electrostatic atomization [44]. In the 1960s, Taylor found that with the increase of voltage, the charged liquid with a certain viscosity gradually formed a hemispherical pendant droplet at the end of the capillary in the process of charge-induced splitting of droplets [37]. With the further accumulation of the surface charge of the droplet, the hemispherical droplet would become conical when the charge repulsion was balanced with the surface tension of the polymer solution; and when the charge repulsion exceeded the surface tension, liquid jets were ejected from the surface of the suspended conical polymer droplet, as shown in Fig. 1b. This pendant conical droplet is called the "Taylor cone". Furthermore, Taylor analyzed the effects of liquid feeding rate, voltage, and distance on the jet stability in the dynamic process of charge-induced splitting of droplets with a certain viscosity, and calculated the half-angle degree of the Taylor cone when the jet formed was 49.3°. The calculation formula of critical voltage (V_c) of jet ejected from the tip of Taylor cone was [45]:

$$V_c^2 = \frac{4H^2}{h^2}\left(\ln\frac{2h}{R} - \frac{3}{2}\right)(1.30\pi RT)(0.09) \quad (1)$$

where H is the working distance between the spinneret and the collector, h is the length of the jet, R is the radius of the nozzle, and T is the surface tension of the solution. For the electrospinning process, the charged polyoxyethylene oxide (PEO) liquid with a certain viscosity would form a Taylor cone at the end of the nozzle, and then jets would be formed on the surface of the Taylor cone (Fig. 1c, d) [38].

When the jet is ejected from the Taylor cone, it would be stretched, thinned, split into finer jets, and finally solidified into polymer fibers. The flight process of jets can be divided into the stable motion zone and unstable motion

zone, as shown in Fig. 1e [39]. In the jet stability zone, assuming that the distance from the end of the nozzle to the end of the stable jet is L, the current on the jet is determined by its resistance, which is mainly composed of the conventional resistance and the resistance generated by the flow of charge in the fluid. The former is related to the charge distribution of the liquid surface; when the jet leaves the tip of the nozzle, the charge on the jet surface is transported along with its mass, and the resistance is controlled by the surface charge and flow rate. When the resistance changes from a region dominated by conventional resistance to a region dominated by charge flow, the distance is exactly L, which can be expressed by Eq. (2) [46]:

$$L = \frac{4kQ^3}{\pi\rho^2 I^2}\left(R_0^{-2} - r_0^{-2}\right) \tag{2}$$

where $R_0 = (2\sigma Q/\pi k\rho E)^{1/3}$, Q is the flow rate, σ is the surface charge of the jet, k is the dimensionless conductivity, E is the electric field intensity, I is the current in the jet, ρ is the liquid density, and r_0 is the initial radius of the jet. By spinning poly(hydroxybutyrate-*co*-valerate) and cellulose solution, the researchers found that the formula was in good agreement with the experimental results [46]. After passing through a short-distance stable region, the jet will enter the unstable region because of the existence of the external electric field and the surface charge of the jets. This instability propagates along the axial direction of the jet and expands continuously, which depends on parameters such as the flow velocity, radius, and surface charge of the jet. Instability includes axisymmetric instability and non-axisymmetric instability. The characteristic of axisymmetric instability is that the axial centerline of the jet does not change but changes in the radial direction. The non-axisymmetric instability is just the opposite, that is, it changes along the axial direction of the jet and does not change in the radial direction (Fig. 1f) [40]. In the unstable region, the jet is further stretched after unstable high-speed movement and finally solidifies into fibers with a diameter of several nanometers to several micrometers with the rapid volatilization of the solvent (Fig. 1g) [39].

Influencing Factors of Electrospun Fibrous Sponges

All the polymer properties, solution properties, processing parameters, and environmental parameters have impacts on the structures of fiber sponges [47–49], these influencing factors are often related and affect each other. The effects of these factors on the morphology and structure of electrospun fiber sponges are briefly discussed below. Polymer molecular weight is a significant parameter influencing electrospun fiber sponges, to be able to prepare fiber sponges, the polymer must have a certain molecular weight and the corresponding solution possess a certain viscosity, otherwise, it is an electrostatic atomization process, and only aerosols or polymer microspheres can be obtained. In addition, the dielectric properties of the polymer have a great impact on the fluffy properties of electrospun fiber sponges (Fig. 2a). Chen et al. found that the negatively charged polymers (cellulose acetate butyrate (CAB), polymethyl methacrylate (PMMA), and polystyrene (PS)) could be spun into fluffy spongy structures better than positively charged polymers (poly($_L$-lactic acid) (PLLA)) under high-voltage electric fields (Fig. 2b) [50]. This is because all the surfaces of electrospun CAB, PMMA, and PS fibers carried negative charges, while the surfaces of PLLA were positively charged. Due to the differences in the polymer properties, the jets were polarized by the induction of a high-voltage electrostatic field during the electrospinning process, resulting in different types of charges on the fiber surface. Since a positive high voltage was applied during spinning, the needle tip was positively charged, which attracted the negatively charged primary fibers to accumulate towards the needle tip, while the fibers carrying the same negative charge tended to repel each other when deposited on the receiving device. The synergistic effect of these two forces resulted in the formation of loose and fluffy fiber sponges in a short time (Fig. 2c).

The main function of the solvent in the spinning solution is to unravel the entanglement between the polymer molecular chains. The physical properties of the solvent have a great impact on the electrospinning process, and then affect the fiber structure of electrospun sponges [51]. Lv et al. investigated the influence of solvent types (*N*,*N*-dimethylformamide (DMF), tetrahydrofuran (THF), and DMF-THF mixture) and ratios on the morphology of PS fibers [52]. When the solvent was DMF, since the vapor pressure of water (2.34 kPa, 20 °C) is greater than that of DMF (0.36 kPa, 20 °C), a solid PS shell layer was first precipitated by non-solvent of water on the jet surface (Fig. 2d). The shell trapped DMF inside and slowed its evaporation rate, water vapor continuously entered the PS-DMF phase through the shell, resulting in rapid phase separation and forming pores inside the fiber. During the penetration of water vapor into the jet, a small portion of the DMF was extruded from the fibers, leaving visible pores on the surface (Fig. 2e). When the solvent was THF, the vapor pressure of THF (19.07 kPa, 20 °C) is higher than that of water. The interface between jet and air was saturated by THF, which hindered the formation of the shell and prevented the water vapor from penetrating the jet and phase separation to form internal pores. Evaporation of THF cooled the surrounding environment, and water vapor condensed at the interface between jet and air. Meantime, the charges on the jet surface were polarized and attracted the agglomerated tiny drops of water, which formed pores on the fiber's surface after drying (Fig. 2f). When the

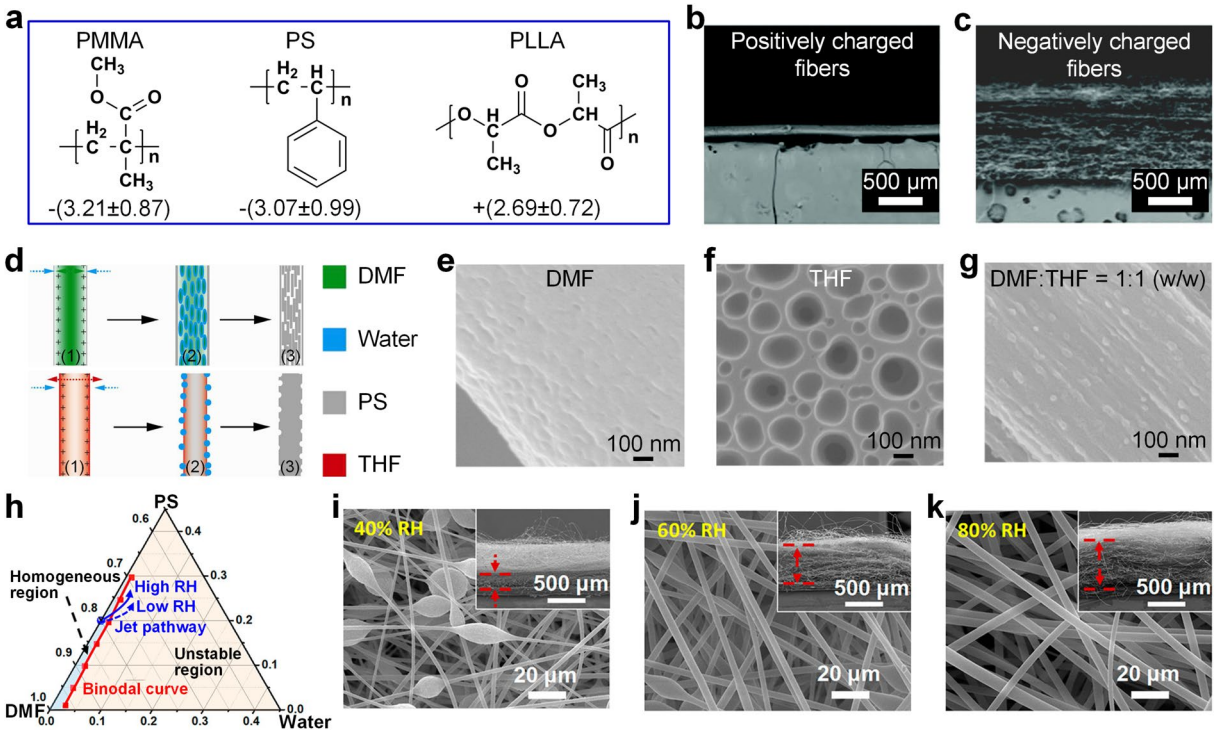

Fig. 2 **a** Structural formulae of PMMA, PS, and PLLA and charge of the resulting fiber sponges after 0.5 h of electrospinning; **b** Dense fibrous membranes obtained by electrospinning of positively charged polymer fibers; **c** Fluffy fibrous sponge obtained by electrospinning of negatively charged polymer fibers; Reproduced with permission from Ref. [50]; Copyright 2019, Royal Society of Chemistry. **d** Schematic diagram of the phase separation process of PS spinning jets with solvents of DMF and THF during flight; Scanning electron microscopy (SEM) image of PS fiber prepared with solvents of **e** DMF, **f** THF, and **g** DMF–THF mixture at a relative humidity (RH) of 42%; Reproduced with permission from Ref. [52]; Copyright 2013, American Chemical Society. **h** Ternary phase diagram of PS–DMF–water system; Surface and cross-section SEM of electrospun PS fiber sponges under different RH of **i** 40%, **j** 60%, and **k** 80%; Reproduced with permission from Ref. [53]; Copyright 2019, American Chemical Society

solvent was a mixture of DMF and THF, the PS shell with high mechanical strength would be formed on the surface to withstand the attack of water vapor without generating some holes on the surface. Then, water vapor penetrated the mixed solvent to cause phase separation to form internal pores, and condensed water accumulated on the fiber surface due to evaporative cooling and charge effect. Although the shell layer can block the violent evaporation of THF, PS-THF solution would remain eject and precipitate into nanopillars at some weak points after encountering surface water droplets (Fig. 2g).

During the electrospinning process, process parameters such as spinning voltage, feeding speed, receiving distance, and environmental conditions would have important impacts on the obtained fiber sponges [54, 55]. These factors often have a certain correlation, and environmental humidity has the greatest impact on the fluffy structure of fiber sponges [56]. Cao et al. constructed a three-phase diagram of the PS/DMF/water system through cloud point titration [53]. As shown in Fig. 2h, the volatilization of solvent during the spinning process under a low-RH environment made the system smoothly cross the binodal curve into the unstable region, and the phase separation speed was slow. On the contrary, in a high-RH environment, the proportion of non-solvent water in the system would greatly increase due to the abundant water vapor in the environment, resulting in the rapid entry of the entire solution into the unstable region and rapid phase separation. Meanwhile, the RH during spinning has a great influence on the morphology of electrospun PS fibers. When the RH was low, a compact fiber membrane with beaded fibers was obtained (Fig. 2i). With the increase in the RH during spinning, the beads on the fibers gradually decreased and fiber aggregate became fluffy (Fig. 2j). When the RH of the spinning environment reached 80%, a fluffy fiber sponge with relatively uniform fibers could be obtained (Fig. 2k). Meantime, the fiber diameter increased with the increase of RH during spinning.

3D Reconstruction of Electrospun Fiber Membranes

3D reconstruction of electrospun fiber membranes includes the homogeneous dispersion and 3D reconstruction of 2D fiber membranes or by special post-processing of electrospun

fibers [25]. At present, the 3D reconstruction methods of electrospun fiber membranes mainly include embedding in hydrogels, 3D printing, gas-foaming, and freeze-drying.

Embedded in Hydrogels

Recently, various types of fibrous sponges have been developed through different composite methods to embed electrospun nanofibers into conventional hydrogels [57, 58], which is a simple method to prepare composite fiber sponges by bonding electrospun fiber membranes with hydrogels. Composite sponges with different structures and applications can be prepared by adjusting the stacking method and the types of nanofibers and hydrogels. As shown in Fig. 3a, electrospun poly($_L$-lactide) (PLA) fiber mesh was impregnated with hydrogel precursor solutions of poly(lactide-*co*-ethylene oxide fumarate) (PLEOF) and hydroxyapatite (HAP) [59], which were then stacked together and compressed. Finally, the multi-layer coating was cross-linked to obtain PLA nanofiber sponges. The tightly bound structure between the nanofibers and the hydrogel endowed the composite sponge with significantly higher Young's modulus than pure PLEOF hydrogel, and the composite sponge showed a promising application prospect in osteogenic differentiation. Furthermore, Poly(caprolactam) nanofiber tubes were prepared by electrospinning nanofibers onto rotating aluminum rods, which were then immersed in a hydrogel precursor solution, followed by cross-linking to obtain nanofiber sponges (Fig. 3b) [60]. A variety of fiber sponges with different shapes can be prepared by manipulating the type of polymer and the inner diameter/shape of the fiber tubes (Fig. 3c). Figure 3d demonstrates that cavity walls of fiber sponge

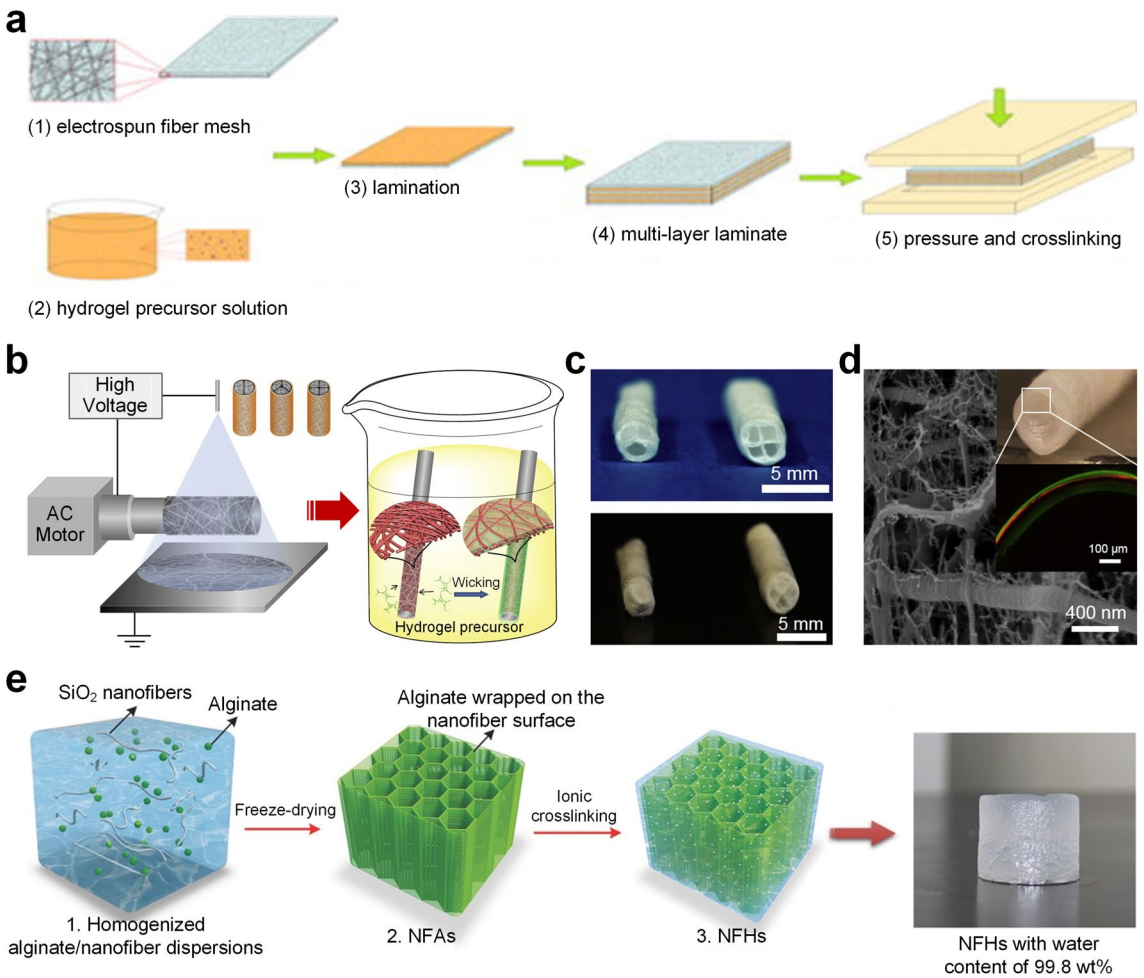

Fig. 3 **a** Schematic diagram of the preparation of fiber sponge obtained by embedding fiber membrane into hydrogel precursor solution; Reproduced with permission from Ref. [59]; Copyright 2010, Elsevier. **b** Schematic diagram of electrospinning collected with tubular receiving device and wicking in hydrogel precursor; **c** Electrospun nanofibrous tubes before and after wicking hydrogel; **d** Image of nanofiber tube and SEM image of the tube wall; Reproduced with permission from Ref. [60]; Copyright 2015, Elsevier. **e** Schematic diagram of the preparation process and optical photos of alginate/SiO_2 nanofibrous sponge; Reproduced with permission from Ref. [61]; Copyright 2017, John Wiley and Sons

exhibited nanofiber network structures, thus endowing it with good mass transfer property. Due to the good biocompatibility of hydrogels and the good mechanical strength of nanofiber membranes, the resulting materials showed good application prospects in the field of cell encapsulation.

In addition, poly(ε-caprolactone) (PCL)/hydrogel composite sponges were obtained by mixing electrospun nanofibers with poly(ethylene glycol)-diacrylate hydrogel macromolecular monomer and following UV crosslinking [62]. The composite sponge could simulate the natural ECM structure, had significant mechanical properties to be injected, and possessed a suitable practical macroscale for relevant clinical tissues, enhancing the biological response of adult stem cells. Recently, a novel porous nanofibrous sponge with ultra-high water content was fabricated by embedding homogeneously dispersed nanofibers in a hydrogel precursor [61]. First, flexible SiO_2 nanofibers were prepared by sol–gel electrospinning, which were dispersed in an alginate aqueous solution to prepare homogeneous nanofiber/alginate dispersion. The dispersion was then freeze-dried in the metal mold and cross-linked by Al^{3+} ions to obtain nanofiber sponges (Fig. 3e). The sponge had zero Poisson's ratio, good durability, rapid resilience (800% min^{-1}), injectability, and shape memory, making it promising for minimally invasive surgery.

3D Printing Method

3D printing is a promising technology that can precisely regulate the shape and porosity of materials [63], but most 3D printing materials lack fibrous surface structure, which limits their application in tissue engineering and other fields. Combining electrospinning technology with 3D printing technology can prepare fibrous sponges with controllable shape and porosity. Mo et al. convert the electrospun gelatin/poly(lactic-*co*-glycolic acid) (PLGA) fiber membranes into short fiber powder by homogeneous dispersion and evaporation drying, and 3D printing ink was obtained by adding the fiber powder into hyaluronic acid (HA) and PEO solution following with stirring (Fig. 4a) [64]. Then, the mechanical properties of the 3D printing sponge were improved by freeze-drying and cross-linking, and sponges could recover their original shape after absorbing water, showing good shape memory properties (Fig. 4b). Moreover, their feasibility of tissue regeneration was further evaluated by cartilage regeneration models in vitro and in vivo. On this basis, the introduction of decellularized ECM into the fiber printing ink endowed the sponge scaffold with better biocompatibility [65]. Owing to the composite advantages of fibrous structure, good elasticity, and biocompatibility, the composite sponge could significantly repair the cartilage defects of rabbits. In addition, a variety of composite sponges were prepared by combining electrospun fibers and 3D printing scaffolds [66–68], which were used in the fields of cartilage differentiation, neural scaffolds, and bone tissue repair.

Recently, Zhang et al. developed the stable jet electrospinning (SJES) method based on ordinary solution electrospinning [69], which eliminated or suppressed the bending instability of spinning jets by changing the viscoelasticity of polymer solution, thereby forming stable polymer solution jets (Fig. 4c). The PLLA/PEO fiber scaffold with 3D patterns could be directly printed by integrating SJES with a programmable translation stage (Fig. 4d, e), which offered an ordered microenvironment to cell culture. On this basis, silk fibroin (SF)/PEO fiber scaffolds with orientation characteristics were further printed [70]. The highly oriented arrangement of the fibers endowed the sponge with good mechanical properties and cell affinity, which provides a basis for the research on anisotropic tissue regeneration.

Gas-Foaming Method

The preparation of fiber sponge by the gas-foaming method is in situ generated bubbles in the fiber membrane through chemical reaction or adding inert gas, thus the tightly packed 2D nanofiber membrane can be reassembled into a fluffy 3D fiber sponge [71–73]. It is a convenient and quick method to use the chemical blowing agent sodium borohydride ($NaBH_4$) to release hydrogen [74–76]. Kim et al. carried out gas-foaming on a variety of electrospun fiber membranes (PCL, Nylon-6, cellulose acetate (CA), and polyvinylidene fluoride (PVDF)), and studied the matching relationship between the polymer polarity and the solvent of $NaBH_4$ [77]. In the process of gas foaming, hydrogen trapped in porous fibrous membranes applied pressure on nearby fibers and rearranged the fibers into sponge structures. In addition, by changing the shape of the fiber membrane or using a custom-made rectangular foaming mold, PCL and polyacrylonitrile (PAN) fiber-based sponges with a tubular shape or precise thickness could be prepared [78–83]. On this basis, to precisely control the shape of the 3D scaffold, He et al. first prepared a hemispherical mold with a 3D printer, cut the 2D electrospun membrane into a circle, and put it into the mold together with the $NaBH_4$ particles (Fig. 5a) [84]. After foaming, the fiber membrane was directly restructured into a hemispherical fiber sponge (Fig. 5b, c). The shape of fiber sponges could be precisely controlled by changing the type of mold. Subsequently, the cells were inoculated on the fiber sponges by 3D bioprinting, and the cells encapsulated in the hydrogel gradually migrated back to the fiber sponges, providing a feasible strategy for the possible deposition of cells on the 3D scaffolds. In addition, the SF/PLA fiber sponge obtained by gas foaming was implanted into a pre-prepared chitosan catheter, and the resulting composite 3D scaffold could be used for nerve tissue repair [75].

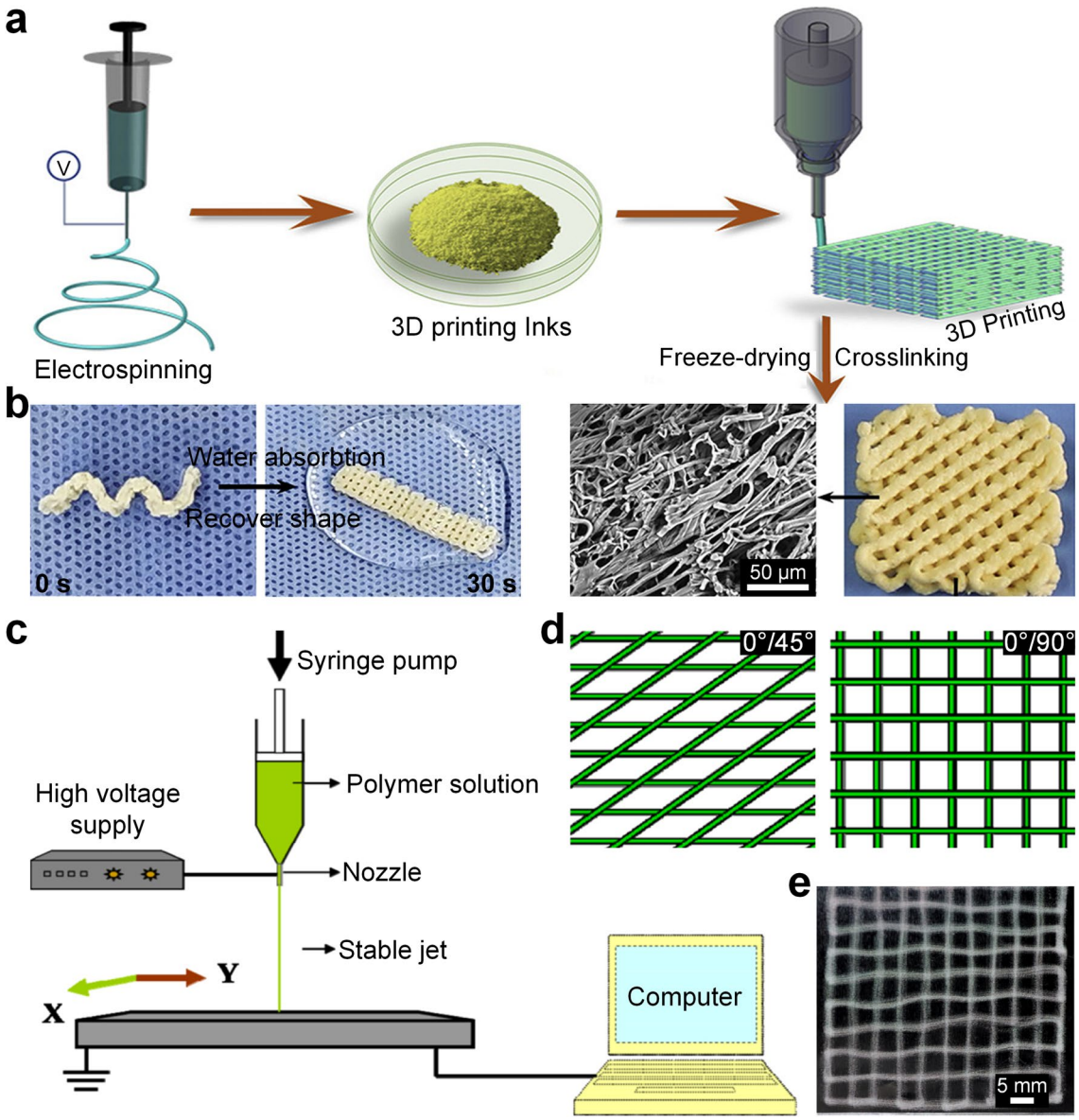

Fig. 4 **a** Schematic diagram of the preparation of 3D printed fiber scaffolds; **b** the fiber scaffolds could quickly return to their original shape after absorbing water; reproduced with permission from Ref. [64]; Copyright 2019, Elsevier. (c) Schematic diagram of a stable jet printing device; (d) programming pattern for printing electrospun fibers; (e) the printed 3D structural fiber sponge with a size of 5 × 5 cm^2; Reproduced with permission from Ref. [69]; Copyright 2015, IOP Publishing

Since using $NaBH_4$ as a blowing agent require to dissolve in water generating hydrogen, it may have side reactions with polymers or encapsulating substances, and is limited to water-insoluble materials. In contrast, carbon dioxide (CO_2) has become a good foaming agent because of its non-toxic, non-flammable, and low cost. Xie et al. expanded the electrospun PCL nanofiber membrane into a 3D sponge scaffold by decompressing the subcritical CO_2, and the thickness of the 3D sponge could be customized by increasing the expansion times and processing time [86]. The fluorescent dye coumarin 6 and antibacterial peptide LL-37 were further introduced into the fiber, endowing the fiber sponge with good fluorescence and antibacterial activity. Mi et al. proposed a new method to prepare fluffy fiber sponges by using the difference in CO_2 solubility of water and ethanol (Fig. 5d) [85]. First, the electrospun PCL fibers were deposited in a 70% ethanol bath, the obtain wet nanofibers were transferred to a dry ice/ethanol bath, and then placed in a room temperature water bath. Many bubbles escaped as CO_2 evaporated, resulting in a fluffy fiber sponge with a porosity of up to 95.3%, much higher than that of a 2D fiber membrane (Fig. 5e, f). Further introducing roughness into

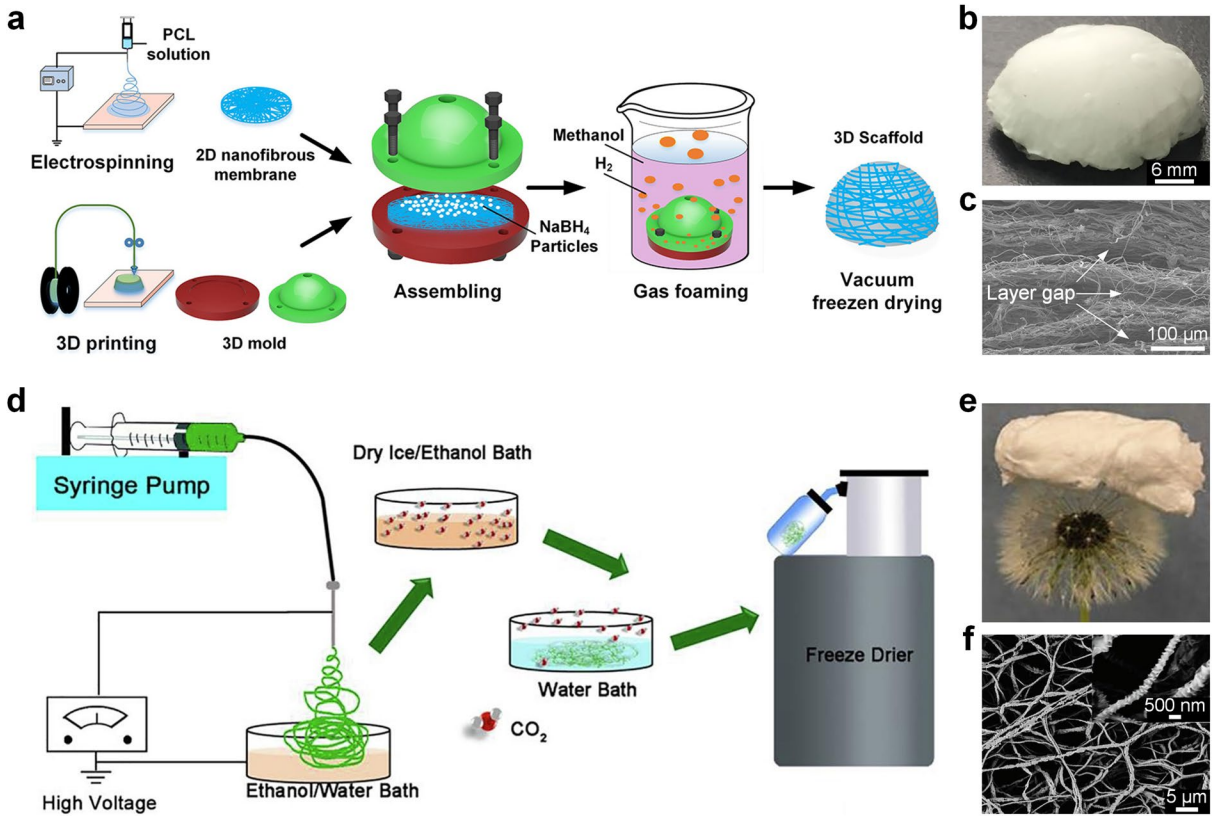

Fig. 5 **a** Schematic diagram of hemispherical 3D scaffold prepared by hydrogen escape method; **b** optical and **c** SEM images of the prepared hemispherical scaffolds; Reproduced with permission from Ref. [84]; Copyright 2018, Elsevier. **d** Schematic diagram of the preparation of 3D PCL fiber sponge by CO_2 escape method; **e** optical and **f** SEM images of 3D fiber scaffold; Reproduced with permission from Ref. [85]; Copyright 2019, Elsevier

the fiber surface increased the cell adhesion and infiltration properties of the material, which has great potential in tissue engineering. Besides, the improved CO_2 escape method can also be extended to other polymer sponges.

Freeze-Drying Method

Although the above methods have realized the preparation of 3D nanofiber materials, they usually require the assistance of other methods, and it is difficult to effectively control the structural characteristics such as the microstructure and pore size. Alternatively, freeze-drying is a commonly used method for preparing aerogels, which generates pores through freezing ice crystals and can effectively retain the pore structure with the sublimation of the dispersion medium during the drying process [87–91]. The resulted fibrous sponges have controllable sizes/shapes and microstructures [32, 92, 93]. Recently, Si et al. first proposed a 3D fiber network reconstruction method combining electrospinning nanofibers with freeze-drying technology, further preparing isotropically 3D nanofiber sponges with tightly bonded fibers [94]. The preparation process of nanofiber sponges mainly included electrospinning, homogeneous dispersion, freeze-drying, and in-situ crosslinking (Fig. 6a). Firstly, electrospun PAN/benzoxazine (BA-a) and SiO_2 fiber membranes were cut into pieces and then added to the dispersing solvent, and the fiber dispersion was obtained by high-speed shearing with a homogenizer. Then, the dispersion was injected into the mold for freezing for 10–30 min, which was transferred to a freeze-drying machine after the dispersion was completely frozen, and fiber aggregates were obtained after 24 h of freeze-drying. Subsequently, stable 3D fiber networks were formed by heating and producing adhesive structures among the fibers, resulting in ultralight and superelastic nanofiber sponges. The freeze-drying method endowed the nanofiber sponges with unique hierarchical network structures (Fig. 6b–e): large pores with an aperture of 10–30 μm and small pores with an aperture of 1–2 μm. The prepared 3D fiber sponges possessed controllable shape/size and good structural tunability, and their minimum bulk density was only 0.12 mg cm^{-3} with porosity as high as 99.992%. This unique bonded network structure endowed the fiber sponge with good mechanical properties, exhibiting good application performance in the fields of thermal,

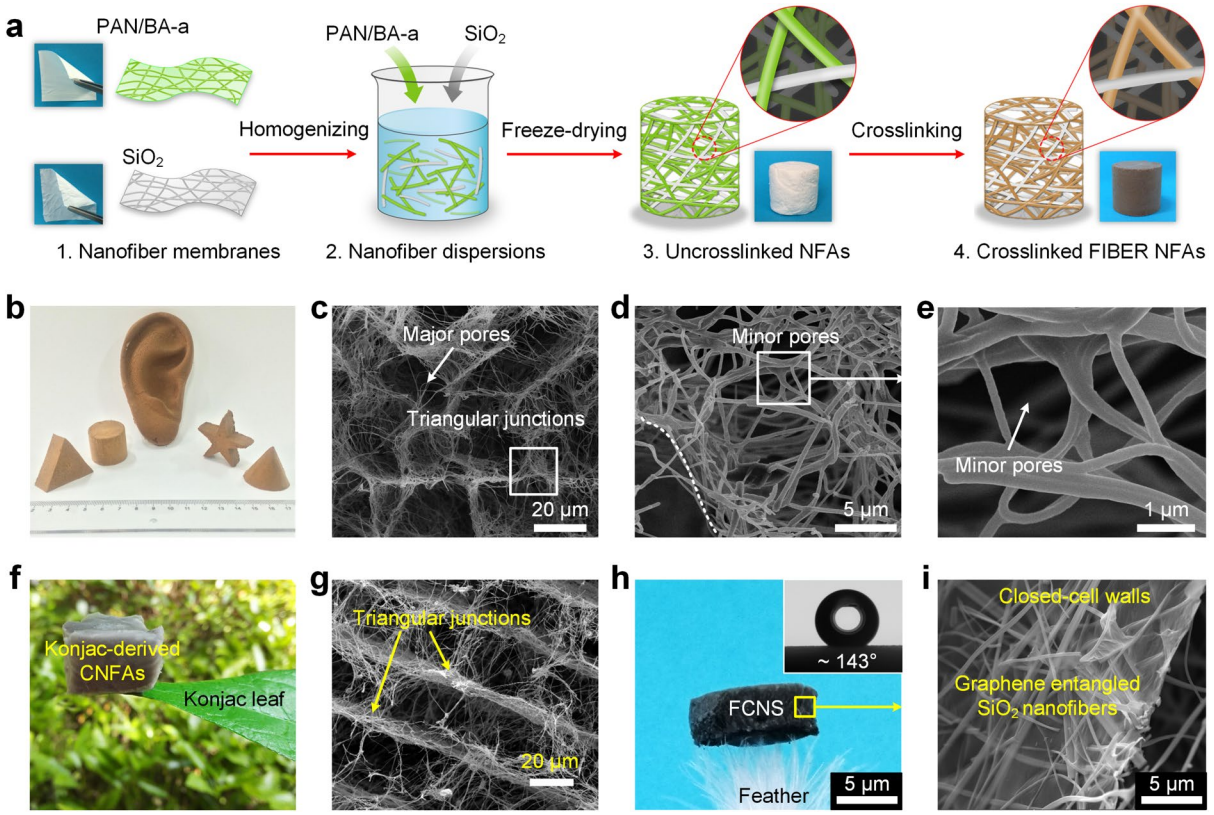

Fig. 6 **a** Schematic diagram of the preparation of PAN/SiO_2 nanofibrous sponges by freeze-drying method; **b** macroscopic optical photos and **c**–**e** microscopic hierarchical SEM images of PAN/SiO_2 nanofibrous sponges; Reproduced with permission from Ref. [94]; Copyright 2014, Springer Nature. **f** Photo showing the ultralight characteristic of carbonaceous nanofiber sponge and **g** its microscopic SEM image; Reproduced with permission from Ref. [106]; Copyright 2016, John Wiley and Sons. **h** Macroscopic and **i** microscopic SEM images of graphene entangled flexible ceramic nanofiber sponge; Reproduced with permission from Ref. [107]; Copyright 2021, Springer Nature

acoustic, electrical, and oil–water separation. Subsequently, various electrospun polymeric, ceramic, and hybrid fiber sponges were successfully constructed by the freeze-drying method [28, 29, 31, 95–105].

On this basis, carbonaceous nanofibrous sponges with adjustable density and shape were prepared by the freeze-drying method using biomass material konjac glucomannan as the carbon source and flexible SiO_2 nanofibers as the skeleton (Fig. 6f) [106]. The obtained sponges have stable cellular structures, and the fibers on the cavity walls are tightly entangled into dense packing states (Fig. 6g), thereby greatly improving the structural stability and mechanical properties of sponges. The hierarchical network structures endowed sponges with ultralight (only 0.14 mg cm^{-3}), super-elasticity (plastic deformation of 4.3% after 1000 compressions), and high-pressure sensing sensitivity. The above-mentioned sponges have good compression properties, but almost no bending properties due to the weaker binding force between the short fibers. To further improve the comprehensive mechanical properties of sponges, bendable and superelastic ceramic nanofiber sponges were constructed by in situ entangling graphene network on the ceramic nanofibers via the directional freeze-drying method (Fig. 6h) [107]. The obtained nanofibrous sponge integrated open macropores, closed-cell walls, and stable entanglement networks (Fig. 6i). On the premise of no chemical cross-linking, the bending and compression performance of sponges were greatly improved through simple physical entanglement, which could be bent 1000 times without structural damage. Meanwhile, the sponges also had good broadband sound absorption performance (noise reduction coefficient up to 0.56). In addition, owing to the scalability of electrospinning technology, some nature-inspired electrospun fiber materials were successfully developed [108], and on this basis, biomimetic nanofibrous sponges were prepared by integrating electrospinning and freeze-drying technique [109]. The obtained electrospun fiber materials show good application prospects in the fields of biosensors and tissue engineering.

Direct Electrospinning of Fibrous Sponges

The above 3D reconstruction method has successfully prepared a series of fiber sponges, but most of them need the assistance of other equipment or methods in addition to electrospinning; thus the preparation process is complicated and the industrial development of materials is limited by complex equipment and methods. In recent years, researchers have also developed fiber sponges with various structures by direct electrospinning, including layer-by-layer stacking method, liquid-assisted collection method, 3D template collection method, particle leaching method, and humidity field regulation method.

Layer-By-Layer Stacking

Stacking the fiber membrane in a certain order by multilayer electrospinning technology is one of the common methods to prepare 3D fiber sponges [23]. 3D PCL fiber sponges with alternating microfibers and nanofibers were prepared by different spinning solutions or by an improved electrospinning device with double parallel spinnerets, which could be used for the culture of different kinds of cells [110]. Moreover, by adjusting the properties of the spinning solution and processing parameters, the researchers also successfully prepared 3D CA sponges with three layers of different structures (Fig. 7a, b) [111, 112]. The combination of electrospinning and other spinning technologies is another method to prepare 3D fiber sponges with layer-by-layer stacking [113–117]. By combining alternant direct polymer melt deposition (DPMD) technology with electrospinning technology, functional 3D fiber scaffolds have been prepared [118]. As shown in Fig. 7c, the microfiber layer was prepared by the DPMD method, and then electrospun PLLA/collagen nanofibers were deposited on the microfiber layer to obtain a fibrous sponge (Fig. 7d). This sponge was composed of PLLA microfiber layers with a fiber diameter of

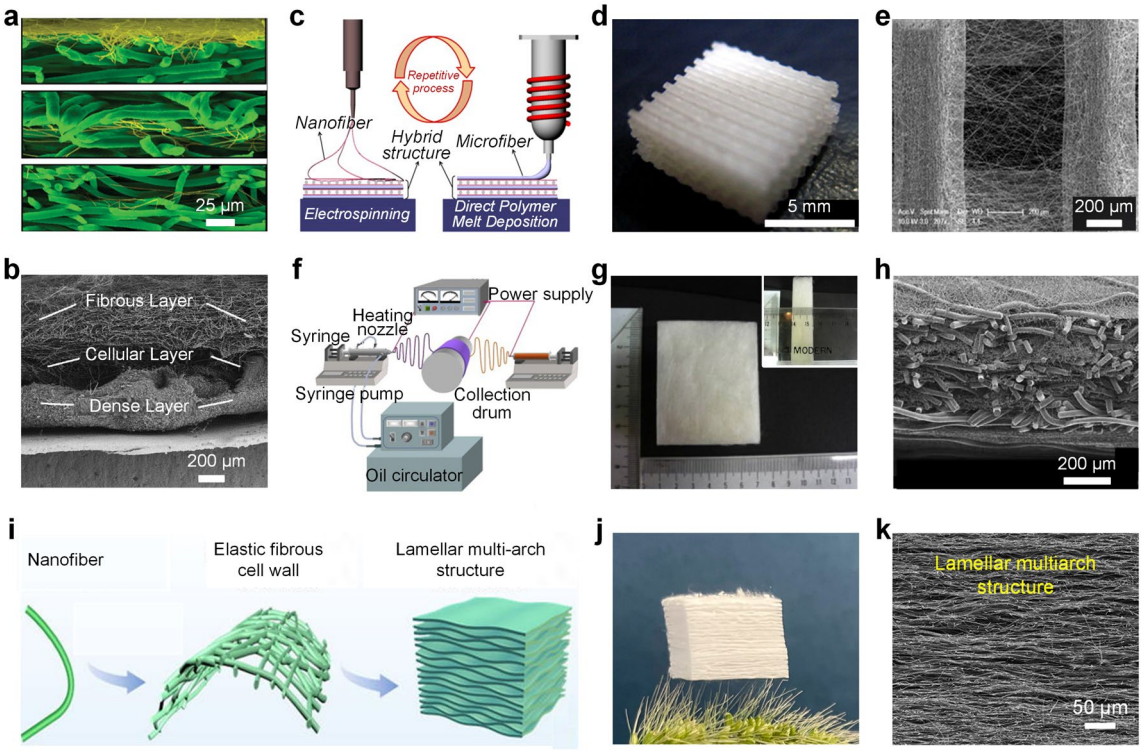

Fig. 7 **a** Cross-sectional SEM images of the PCL micro/nanocomposite fiber sponge prepared by alternating electrospinning; Reproduced with permission from Ref. [111]; Copyright 2006, American Chemical Society. **b** SEM image of multi-layer structured CA fiber sponge; Reproduced with permission from Ref. [112]; Copyright 2006, Elsevier. **c** Composite scaffolds containing PCL microfibers and nanofibers were constructed by alternant DPMD and electrospinning; **d** macroscopic pictures and (e) microscopic SEM images of the PCL micro/nanofiber sponge with a size of 9 × 9 × 3.5 mm^3; Reproduced with permission from Ref. [118]; Copyright 2008, Elsevier. **f** Schematic diagram of hybrid electrospinning device; **g** Macro and **h** microstructure of PLGA nano/microfiber composite sponges; Reproduced with permission from Ref. [119]; Copyright 2010, Elsevier. **i** Schematic diagram of the preparation of ZrO_2–SiO_2 nanofiber sponges; Reproduced with permission from Ref. [120]; Copyright 2022, Elsevier. **j** Lightweight characteristics of ZrO_2–SiO_2 nanofiber sponges; Reproduced with permission from Ref. [121]; Copyright 2022, American Chemical Society. **k** Lamellar multi-arch structure of ZrO_2–Al_2O_3 nanofiber sponges; Reproduced with permission from Ref. [122]; Copyright 2020, American Chemical Society

350 μm and nanofiber layers with a fiber diameter of 325 nm (Fig. 7e). Furthermore, 3D PLGA nano/microfiber sponges with a thickness of 2–3 cm were prepared by combining the solution electrospinning technology with the melt electrospinning technology (Fig. 7f, g) [119]. The 3D sponge was composed of PLGA microfibers (average diameter of 28 μm) and PLGA nanofibers with an average diameter of 530 nm (Fig. 7h). Compared with pure PLGA microfiber scaffolds, the prepared nano/micro composite fiber scaffolds have higher adsorption, diffusion, and filtration performance on human keratinocytes and fibroblasts.

Stacking the nanofiber membranes by post-processing technology is another method for preparing layer-by-layer stacking 3D fibrous sponges [123]. For example, the electrospun nanofiber membrane was cut into small pieces, and fibrin glue or adhesive was injected between the nanofiber layers to maintain the 3D structure of the sponge [121, 122, 124]. Zhang et al. cut the electrospun ZrO_2–SiO_2 nanofiber membranes into predetermined sizes and immersed them in the silica sol, then stacked the fiber membrane layer by layer, frozen, and freeze-dried for 40 h, and then cross-linked multilayer fiber sponges were obtained by calcining (Fig. 7i, j) [120, 121]. The material had lamellar multi-arch structures (Fig. 7k) with compressive strength under 90% strain as high as 950 kPa, and it had temperature-invariant elasticity from −196 to 1100 °C [120, 122]. In addition, 3D nanofiber sponges could also be prepared by electrospinning technology assisted by other devices such as mechanical winding [125, 126].

Liquid-Assisted Collection

Depositing electrospun fibers directly into a collection bath (water, organic solvent, etc.) can obtain nanofiber sponges with different structures by using the resistance or traction of the liquid. Teo et al. deposited electrospun PCL/collagen fibers in inclined and swirling water flow and preliminarily obtained fiber sponges with a certain fluffy degree and thickness by using the guidance and dispersion of water flow (Fig. 8a) [127]. Other researchers have also used similar methods to obtain 3D nanofiber sponges with different stacking structures such as rings and spindles. To obtain 3D fiber materials with higher bulkiness and porosity, organic solvents with lower surface tension (such as ethanol, methanol, tert-butanol, etc.) were used as receiving baths. On this basis, researchers have successfully prepared various polymer sponges (such as SF [128], polyvinyl alcohol (PVA) [129], PCL [130, 131], PVDF [132, 133], polyvinyl acetate [132], PAN [132], PLGA [134], poly(glycolic acid) [135]) and organic–inorganic composite sponges (such as PLLA/vaterite composite sponges [136]). Hong et al. prepared 3D PCL micro/nanofiber sponges with controllable size by depositing electrospun PCL nanofibers in ethanol (Fig. 8b) [130]. By adjusting the flow rate of ethanol and spinning process parameters, the width and height of the 3D fiber structures could be controlled at the centimeter scale (Fig. 8c). Recently, Kasuga et al. proposed a method for the preparation of electrospun cotton-like PLLA/siloxane-containing vaterite composites by receiving fibers in an ethanol bath, and the thickness of the prepared cotton-like sponges was about 40–50 mm [136], as shown in Fig. 8d. By impregnating the surface of the fiber skeleton, calcium phosphates could be deposited on the surface of the material (Fig. 8d inset), which could enhance the adhesion between cells and promote the regeneration of bone tissue.

To effectively simulate biological tissue, it is necessary to precisely control the shape and size of sponges. Chakrapani et al. prepared 3D electrospun PCL/HAP fiber sponges by a dynamic liquid collector with a mixture of isopropanol (IPA) and water, and polytetrafluoroethylene-coated magnetic balls were installed in a bowl container with a metal base (Fig. 8e, f) [137]. The composite sponges possessed a reasonably hierarchical structure suitable for critical defects in the craniofacial region. Moreover, Zheng et al. received electrospun PAN nanofibers by using graphene oxide (GO) dispersions with different concentrations as a collection bath, followed by freezing and freeze-drying for a certain time to obtain fiber sponges with controllable size and shape (Fig. 8g) [138]. Then, hydrophobicity carbon nanofiber/graphene sponges with low density (2–3 mg cm^{-3}) were obtained by following heating and reduction, which can effectively absorb a variety of oils (Fig. 8h). Nevertheless, the disadvantage of the liquid collection is that additional treatment process such as freeze-drying is often required to remove the liquid after electrospinning, which increases the preparation time and cost.

3D Template Collection

3D templates of different shapes and sizes, including metal tubes, metal rings, triangular cones, and meshes, are also used as fiber collectors [139, 140]. By changing the distribution of the surrounding electric field, the charged jet moves directionally, so that the fibers are regularly deposited on the 3D template, and the nanofiber sponge can be obtained after removing the template. Zhang et al. fabricated fiber tubes using a 3D receiver to collect nanofibers by adjusting the electric field force and electric field intensity (Fig. 9a) [141]. The single tubes had multiple microscopic patterns and multi-level connected structures, and their size, shape, structure, and pattern could be adjusted within a certain range (Fig. 9b). The research showed that the distance between the 3D receivers was the main factor, if the distance between the two receivers was too close, the fibers would overlap. Park et al. used a metal ring with a diameter of 38 mm as a receiver, and the fibers were deposited into the

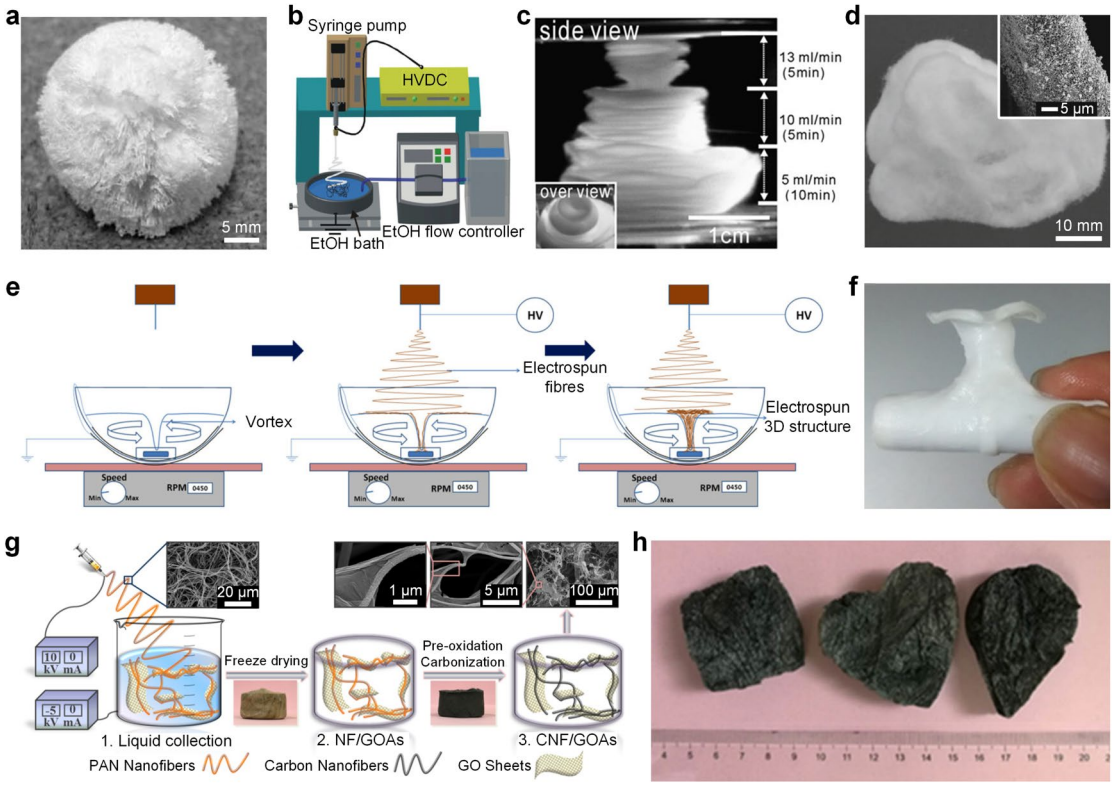

Fig. 8 **a** PCL/collagen fiber sponge prepared with water as the receiving bath collector; Reproduced with permission from Ref. [127]; Copyright 2008, Bentham Science Publishers. **b** Schematic diagram of the electrospinning device with ethanol as the receiving bath collector; **c** PCL fiber sponge prepared with different flow rates of ethanol receiving bath collectors; Reproduced with permission from Ref. [130]; Copyright 2011, Springer Nature. **d** PLLA-based fiber sponge prepared by methanol receiving bath collector (inset is the SEM image of fibers in PLLA-based fiber sponges prepared by alternate soaking); Reproduced with permission from Ref. [136]; Copyright 2012, Springer Nature. **e** Schematic diagram of the preparation of electrospun PCL/HAP fiber sponge using IPA aqueous solution as receiving bath collector; **f** PCL/HAP fiber sponges prepared by changing the content and rotation speed of the receiving bath; Reproduced with permission from Ref. [137]; Copyright 2017, Springer Nature. **g** Schematic diagram of the preparation of PAN fiber-based sponge with GO aqueous dispersion as coagulation bath collector; **h** Prepared GO/carbon nanofiber sponges with different shapes; Reproduced with permission from Ref. [138]; Copyright 2019, Elsevier

ring under the action of electric field force, forming a 3D PS nanofiber sponge with a certain thickness [142]. The interweaving structures of internal fibers endowed the sponge with good mechanical stability. Meanwhile, the material had a high specific surface area, porosity, and open-cell connected structure, showing great potential in the field of supercapacitors.

Based on the above works, Chang et al. took a hollow plastic sphere as a template, and two polyvinyl pyrrolidone (PVP) jets with opposite charges were ejected by using symmetrically distributed voltages of + 12.5 and −12.5 kV [143]. The two kinds of jets attracted each other, collided, and interwoven in the middle plane, and finally the positive and negative charges were neutralized (Fig. 9c). Meanwhile, an adjustable heat source was used to generate controllable upward airflows to balance fiber gravity, resulting in 3D PVP nanofiber sponges (Fig. 9d). Compared with commercial muffler materials, sound absorption coefficients of PVP nanofiber sponge in a frequency range of 400–900 Hz were significantly improved. Feng et al. made a special collector by embedding a group of stainless steel probes with a length of 1.5 cm in a hemispherical plastic disk (8 cm in diameter and 0.2 cm in shell thickness), so that nanofibers were deposited in the center of the plastic disk into a fluffy structured PLLA fiber sponge (Fig. 9e, f) [144]. Subsequently, the fiber sponges were immersed in biomineralized body fluids and freeze-dried to obtain HAP-encapsulated PLLA fiber sponges, the interconnected pores of 65 μm formed between the fibers significantly promoted the culture of human mesenchymal stem cells (hMSCs). The 3D template method can effectively control the macroscopic stacking size and structure of 3D nanofiber materials to a certain extent.

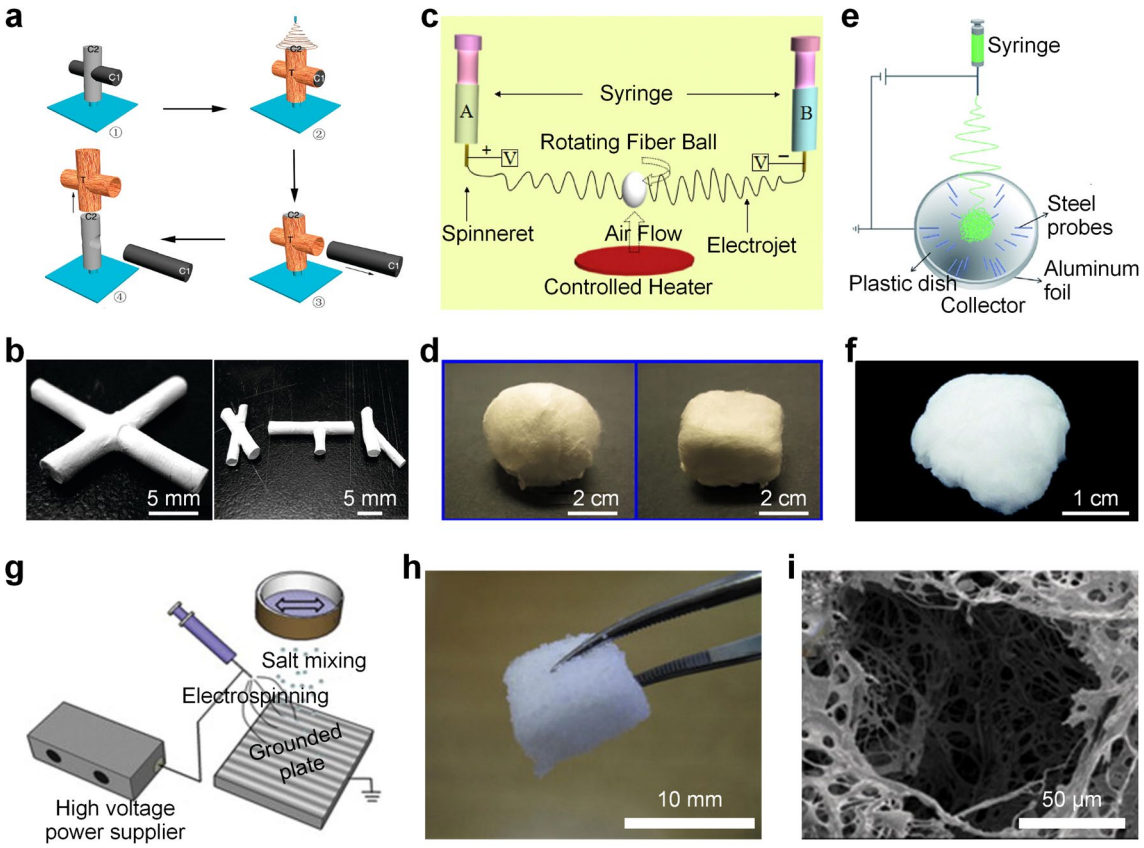

Fig. 9 **a** Schematic diagram of detachable interconnected tubular structures; **b** the prepared interconnecting fiber tubes with different structures; Reproduced with permission from Ref. [141]; Copyright 2008, American Chemical Society. **c** Schematic diagram of preparation device for 3D PVP nanofiber sponges; **d** 3D PVP nanofiber sponges with different geometric shapes; Reproduced with permission from Ref. [143]; Copyright 2016, Elsevier. **e** Schematic diagram of the preparation of PLLA fiber sponge and **f** its macrostructures; Reproduced with permission from Ref. [144]; Copyright 2014, Royal Society of Chemistry. **g** Schematic illustration of the preparation of HA/collagen fibrous sponge by combining electrospinning and salt deposition; **h** photograph of the nanofiber/salt composite scaffold and **i** SEM image of the dried sponge after salt particle removal; Reproduced with permission from Ref. [145]; Copyright 2008, Elsevier

Particle Leaching Method

The main challenge for the preparation of 3D structured electrospun materials is that the deposition characteristic of nanofibers leads to the formation of 2D membranes, to overcome this defect, nanofibers need to be deposited in the 3D direction. Generally, salt particles and ice crystals were used as porogen to prepare 3D nanofiber materials combined with electrospinning technology, and then 3D porous sponges were obtained after removing the porogen. Kim et al. prepared a HA/collagen nanofibrous scaffold containing salt particles by combining electrospinning technology with an automatic vibrating sieve method (Fig. 9g) [145]. Then, salt particles were dissolved in water to prepare nanofibrous sponges with random opening microporous structures (Fig. 9h, i). In addition, the sponges could still maintain a good microporous structure (size of 50–100 μm) after swelling treatment. Another method is to cool the receiving device below the freezing point of the spinning solution so that the ice crystals are rapidly deposited on the surface of the collected fibers, and 3D fiber sponges could be finally obtained after the removal of ice crystals. Schneider et al. added amorphous tricalcium phosphate (TCP) nanoparticles to electrospun PLGA solution and cooled the receiving device with dry ice, resulting in the formation of ice crystals among the fibers [146]. By sublimating the dry ice, PLGA/TCP fiber sponges were finally obtained with a porosity of 95% and a fiber diameter of 5–10 μm.

Although the above method can prepare 3D fiber material, the preparation method is complicated and the added particles are easy to remain. Recently, it has been found that fibrous sponges can also be prepared by introducing small molecular monomers or polymers into electrospinning [147]. Park et al. added lactic acid (LA) into PLA solution, and then β-TCP particles were added into the mixed solution for electrospinning [148]. Many charged groups (COOH) in LA lead to charges repulsive between fibers to form a 3D fiber scaffold. Then the scaffold was immersed in distilled water

to leach lactic acid, and PLLA/β-TCP fibrous sponges were obtained by following freeze-drying, which had a swelling rate 2.5 times higher than that of 2D fibrous membranes, opening up a new way to manufacture 3D fiber scaffold with biological activity. Jang et al. performed coaxial electrospinning of PS (shell layer) and PCL (core layer) solution, and electrons in the PS shell moved freely through residual solvent and generated electrical repulsion to surrounding fibers, and thus the composite sponges were formed [149]. After soaking in DMF, the PS shell layer was selectively dissolved by the difference in solubility of the two polymers in DMF, and PCL fiber sponges were prepared. Further introduction of dopamine improved the mechanical stiffness of PCL fiber sponge, showing great application potential in tissue engineering scaffolds and drug delivery carriers.

Humidity Field Regulation

Environmental humidity is the main factor affecting the solidification and charge dissipation of electrospun fibers. 3D nanofibrous materials with different stacking structures can be easily prepared by adjusting the environment humidity without the assistance of external devices. Ke et al. dissolved CAB in dual solvents with different ratios of dichloromethane and DMF, and then electrospun fibers were deposited on a collector including a humidification system and solution irrigation (Fig. 10a) [50]. Then, CAB fiber sponges were prepared by adjusting the wind speed of the humidifier during the spinning process, and the volatilization of the highly volatile solvent bonded the as-spun fibers to each other (Fig. 10b, c). The obtained sponge showed great application advantages in the fields of oil–water separation and air filtration. In addition, this method can also be extended to various polymer fiber sponges such as PMMA, PS, and PLLA. Cheng et al. prepared electrospun CA fibers by adjusting the RH and found that the 3D fluffy structure can be obtained when the RH exceeded 60% [150]. This is because the high RH environment can accelerate the solidification of the jet so that the jet can solidify before reaching the receiving plate. Meanwhile, a large amount of residual electrostatic charge on the fiber increased the electrostatic repulsion between the fibers, and nanofiber sponges can be accumulated in a short time. Kim et al. also prepared PVDF/barium titanate/multiwalled-carbon nanotubes composite

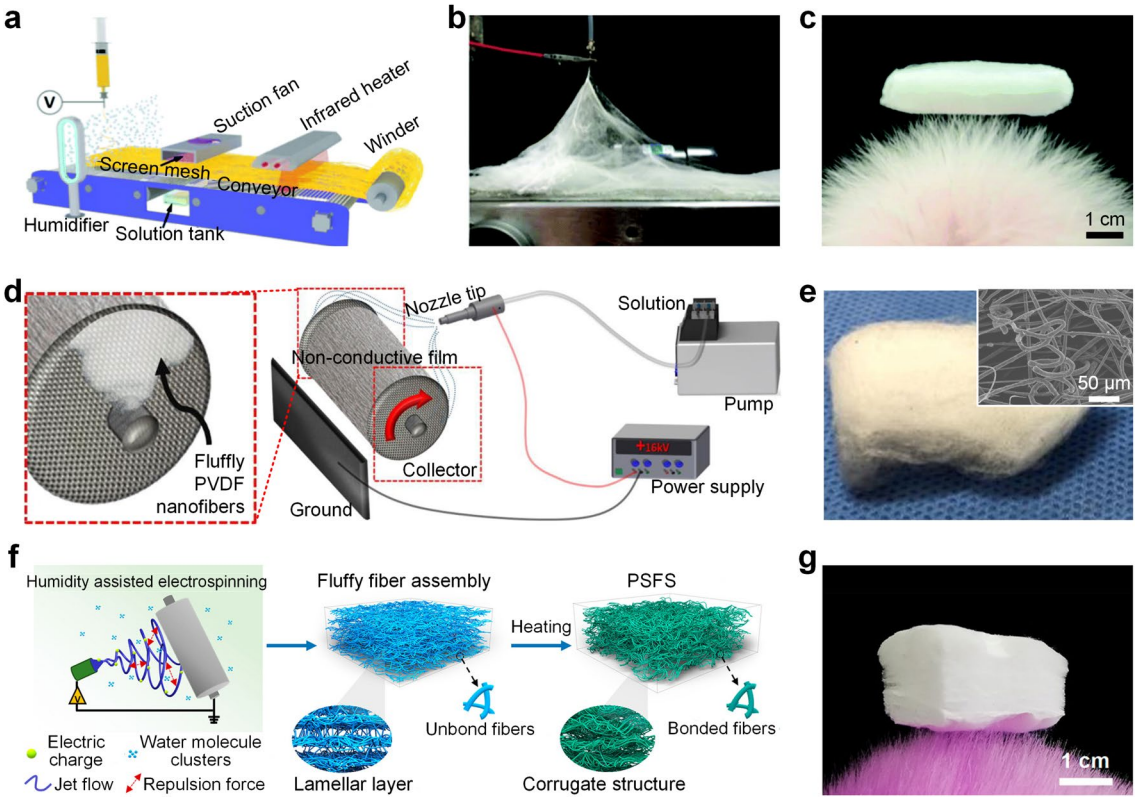

Fig. 10 Schematic diagram of **a** preparation device and **b** preparation process of CAB fiber sponge; **c** optical photo of the prepared CAB fiber sponge; Reproduced with permission from Ref. [50]; Copyright 2019, Royal Society of Chemistry. **d** Schematic diagram of electrospinning for preparing 3D PVDF fiber sponge; **e** macro and microstructure pictures of 3D PVDF fiber sponge; Reproduced with permission from Ref. [151]; Copyright 2019, Elsevier. **f** Schematic diagram of the preparation process of PS fiber sponge; **g** ultralight properties of PS fiber sponge; Reproduced with permission from Ref. [53]; Copyright 2019, American Chemical Society

fiber sponges by studying the effect of RH on the fluffy structure of fibers (Fig. 10d) [151]. When the RH was less than 60%, the lap points between fibers would be partially melted and the fibers would be closely stacked into a 2D membrane. By contrast, high electrostatic repulsion between spinning jets facilitated the formation of 3D fibrous sponges when the RH was increased to 90% (Fig. 10e).

The above-mentioned method based on humidity regulation successfully realizes the preparation of fiber sponge, but the sponge lacks effective bonding points due to the fluffy accumulation between fibers, resulting in poor mechanical properties. Aiming at the problem of poor structural stability of the current electrospun fluffy fiber materials, Cao et al. prepared a fluffy PS fiber aggregate by regulating the RH, studied the effect of RH on PS fiber and fiber aggregate, and analyzed the forming mechanism by phase separation of fluffy fiber (Fig. 10f) [53]. On this basis, electrospun fiber sponges with multi-layer corrugated microstructures were obtained through subsequent thermal crosslinking by in situ introducing crosslinking agent trimethylolpropane tris (2-methyl-1-aziridine propionate) (TTMA) into PS solution (Fig. 10g). The crosslinked fiber network and layered corrugated structure could effectively disperse the stress of the material during compression and improve the mechanical stability of the sponge, and its plastic deformation was only 11% after 100 compressions with the 60% strain. Besides, the electrospun fiber sponge also has good low-frequency sound absorption performance with a density of only 6.63 mg cm^{-3}, showing lightweight features. Subsequently, a series of fiber sponges such as polysulfone (PSU), polyphenylsulphone (PPSU), and PMMA with good mechanical properties were successfully prepared by similar methods [152–159].

Applications of Electrospun Fibrous Sponges

Sound Absorption

Electrospun fiber sponges, with their controllable thickness and volume density, meet the requirements of high efficiency and broadband sound absorption [27]. On the one hand, the thickness plays an important role in improving the sound absorption performances of fiber materials, relatively large thickness can effectively prolong the dissipation path of sound waves, thus enhancing the dissipation of sound energy. Meanwhile, the high porosity of fiber sponges reduces the surface acoustic impedance, allowing more sound waves to enter and dissipate continuously [160]. On the other hand, fiber sponges possess a small fiber diameter and high specific surface area, thus increasing contact points and friction resistance between fibers and sound waves, so that the sound energy is converted into heat energy and attenuated [161]. Chang et al. obtained 3D electrospun PVP nanofiber sponges with fluffy structures by two nozzles loaded with opposite voltages and used air flow-assisted reception in the middle of the two nozzles [143]. The sound absorption performance of the PVP nanofiber sponges in the frequency range of 200–1600 Hz was significantly better than that of traditional cotton fiber aggregates. However, this method is complicated to operate, and the structural stability of the fiber sponge is poor due to the simple stack of fluffy fibers. Recently, Cao et al. obtained ultra-fine PS fiber aggregate through RH induction in the electrospinning process by using TTMA as the cross-linking agent, and the fiber sponges with multi-layer corrugated microstructure were achieved through subsequent crosslinking treatment (Fig. 11a) [53]. The multi-layer fiber structures in the sponge enabled the sound waves to be repeatedly transmitted and reflected between the layers, endowing it with good sound absorption performance in the low-frequency band (Fig. 11b). The sound absorption coefficient of PS fiber sponges at 1000 Hz was as high as 0.9, and they could still maintain good sound absorption performance in a high RH environment (Fig. 11c). However, due to the single structure of the sponge, its high-frequency sound absorption coefficient decreased.

On this basis, Feng et al. prepared PSU/PVDF fiber sponges by blending electrospinning, and then PSU/PSU-PVDF/PVDF composite fiber sponges were achieved by gradually changing the RH (Fig. 11d) [153]. The gradient structure composed of a fluffy layer/blend layer/dense layer in the sponge effectively improved the sound absorption performance of the material. The fluffy layer toward the sound source allowed more sound waves to enter and dissipate continuously, and the gradually decreasing pore size made it difficult for sound waves to transmit from the sponge so that they were constantly reflected and dissipated in the sponge, and the noise reduction coefficient of the sponge reached 0.53 (Fig. 11e, f). To further improve the sound absorption coefficient while maintaining the light weight of the material, inspired by the characteristics of low-density materials with good high-frequency sound absorption and high-density materials with good low-frequency sound absorption properties. Zong et al. constructed sandwich-structured fiber sponges with a low–high–low density by directional freeze-drying and entanglement crosslinking methods (Fig. 11g) [107]. The low-density unit made the sound waves easy to enter, and then gradually dissipated ultra-broadband sound waves through the high- and low-density units, and the noise reduction coefficient reached 0.56 (Fig. 11h). In addition, the sandwich-structured sponge could reduce the white noise from 80 to 53 dB, and the sound absorption performance is far better than that of commercial fiber felt while maintaining lightweight (Fig. 11i).

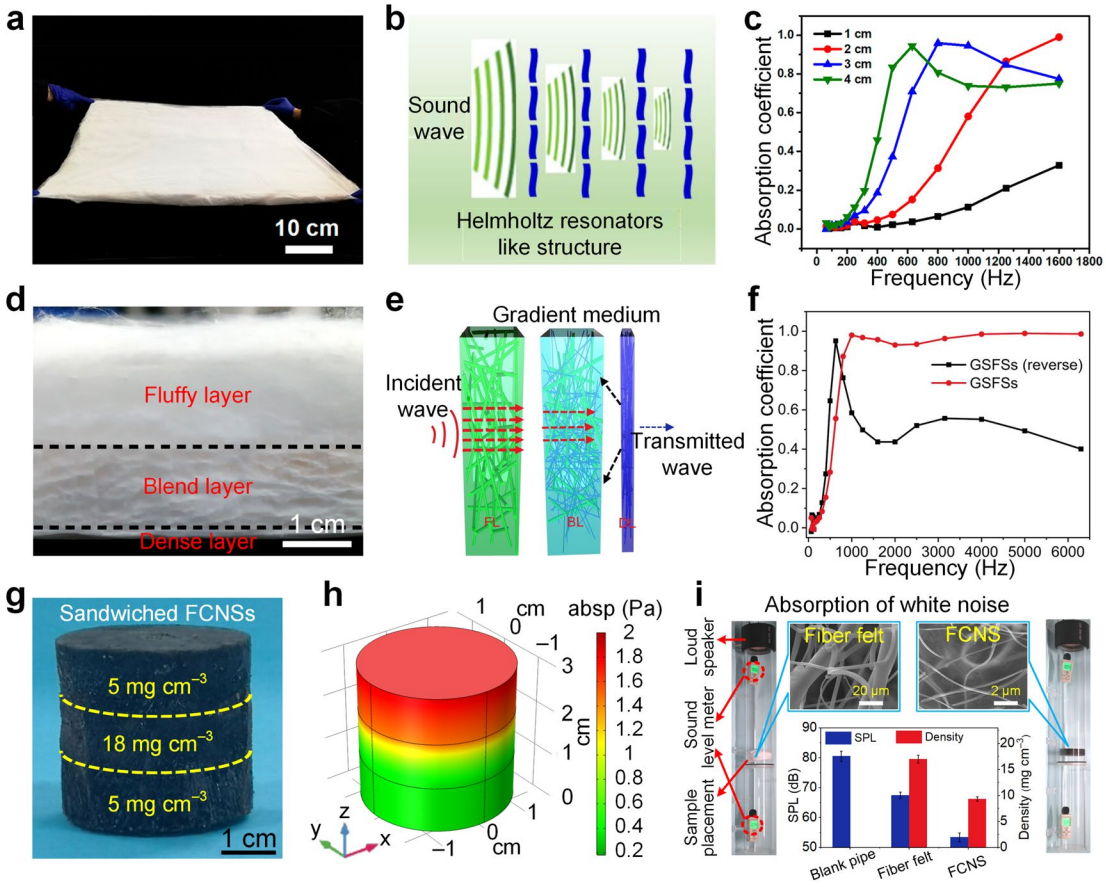

Fig. 11 **a** Optical photo of PS fiber sponge with a large size 60×70×1.5 cm^3; Schematic diagram of **b** sound energy dissipation and **c** sound absorption performance of PS fiber sponge; Reproduced with permission from Ref. [53]; Copyright 2019, American Chemical Society. **d** Gradient fiber sponges with a three-layer gradient density structure; **e** Schematic diagram of the sound energy dissipation principle and **f** sound absorption performance of the gradient structured fiber sponge; Reproduced with permission from Ref. [153]; Copyright 2021, Elsevier. **g** Macro photo of sandwich-structured nanofiber sponge; **h** sound pressure distribution and **i** practical sound absorption applications of sandwich-structured nanofiber sponges; Reproduced with permission from Ref. [107]; Copyright 2021, Springer Nature

Warmth Retention

Electrospun fiber sponges have a small diameter and high specific surface area, which could divide air in the fiber sponge into numerous tiny pores to store more still air and reflect human radiation efficiently. Compared with ordinary fibers, it has more efficient warmth retention performance under the same weight and has become an important trend in the development of lightweight and efficient warmth retention materials [158]. Wu et al. constructed micro/nanofiber composite sponges by freeze-drying method, taking flexible PAN nanofibers and rigid polyester (PET) microfibers as frameworks (Fig. 12a) [100]. Meanwhile, water-based crosslinking agents and hydrophobic agents were introduced into the fiber dispersion, endowing fiber sponges with elastic and washable properties. The obtained micro/nanofiber sponge had good structural stability, and its plastic deformation was only 5.7% after 1000 cycles of compression with a strain of 60%. Moreover, the introduction of microfibers resulted in a tortuous micro-pore structure inside the fiber sponge, endowing the material with low thermal conductivity (28.51 mW m^{-1} K^{-1}) at a low density (7.5 mg cm^{-3}) (Fig. 12b). In addition, the prepared sponge also had water-washing invariant hydrophobicity and stable long-term warmth retention (Fig. 12c). However, the preparation process of the micro/nanofiber sponge involves the preparation of electrospun nanofiber, homogenization of micro/nanofiber composite dispersion, freezing, vacuum drying, and heating crosslinking, suffering from long time and high energy consumption.

To simplify the preparation process of warmth retention materials, Wu et al. prepared fiber aggregates by electrospinning the mixed solution of PS and PU in a high RH environment [159]; then, PS/PU fiber sponge was obtained by adding crosslinking agent TTMA to the spinning solution and subsequent heating treatment. The sponge had

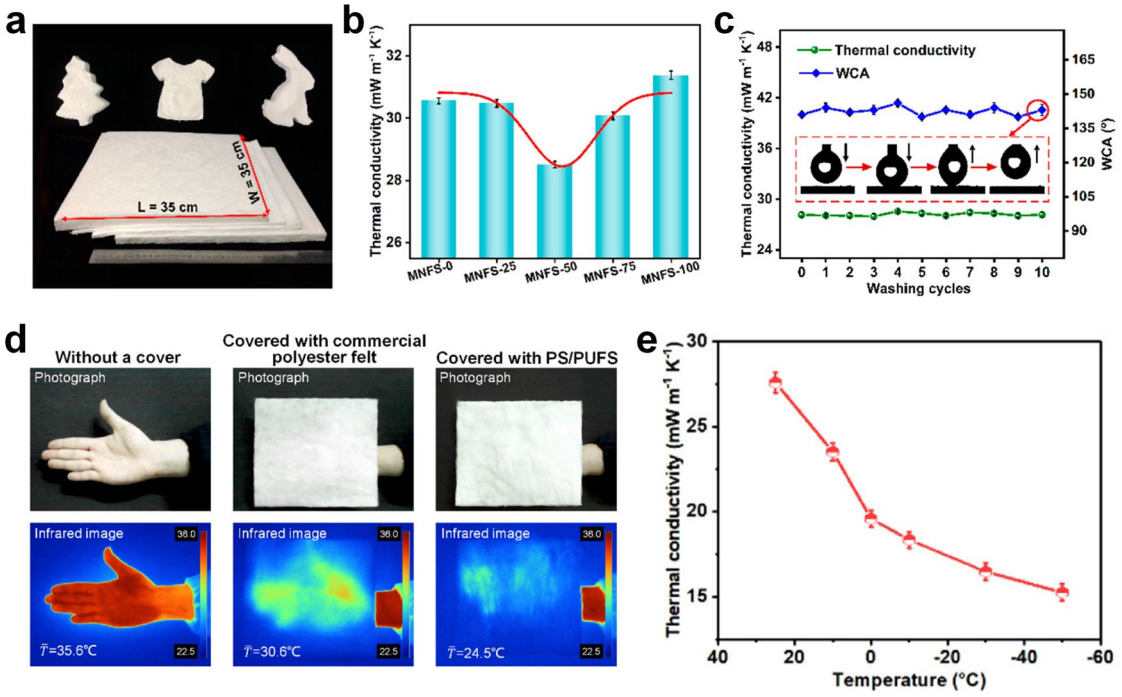

Fig. 12 **a** Optical pictures of various shapes of micro/nanofiber sponges; **b** thermal conductivity of sponges prepared with different ratios of micro and nanofibers; **c** thermal conductivity and water contact angle of micro/nanofiber sponges after different washing cycles; Reproduced with permission from Ref. [100]; Copyright 2022, American Chemical Society. **d** Comparison of warmth retention performance between PS/PU fiber sponge and commercial PET fiber felt; **e** thermal conductivity of PS/PU fiber sponge at different temperatures; Reproduced with permission from Ref. [159]; Copyright 2020, American Chemical Society

good mechanical properties, its plastic deformation was 4.9% after 100 compressions at 50% strain, and the tensile fracture stress and elongation reached 367 kPa and 70%, respectively. Subsequently, the prepared PS/PU fiber sponge and commercial PET microfiber felt were placed on the same palm respectively, as shown in Fig. 12d, the surface temperature of the palm covered by the PET microfiber felt was 30.6 °C; while when the fiber sponge was placed above the palm, the mean temperature of palm was only 24.5 °C, indicating its efficient warmth retention performance. In addition, the thermal conductivity of obtained fiber sponge was only 27.6 mW m^{-1} K^{-1} at 25 °C, and the thermal conductivity decreased as the test temperature decreased (Fig. 12e), indicating that the material had high warmth retention performance at low temperatures. Subsequently, PSU/PU fiber sponges were prepared by a similar method, the high porosity and small fiber diameter endowed PSU/PU sponge with low thermal conductivity of 25.8 mW m^{-1} K^{-1} [162]. Further introduction of thermally stable polymers (polyamic acid [154] and polyamide-imide (PAI) [157]) or small molecules (ZrC nanoparticles [152] and phosphonic acid flame retardants [156]) in the spinning solution endowed sponges with good flame retardant and active warmth retention performance.

Thermal Insulation

The interpenetrating network structures of fibrous sponges endow them with small pore size, high porosity, high pore tortuosity, and large specific surface area, resulting in long and complex heat conduction path and enhanced heat dissipation [98, 163, 164]. Meanwhile, it can also restrict the movement of gas molecules in the sponge, and thus effectively suppress the heat transfer and convection of the gas phase, showing broad application prospects in the fields of thermal insulation. Si et al. prepared ultralight and superelastic ceramic nanofiber sponge with laminar cellular structure by using flexible SiO_2 nanofibers as building blocks and aluminoborosilicate as a binder, which showed temperature-invariant superelasticity in the range of −100 to 500 °C [29]. In addition, the thermal conductivity of the sponge (density of 10 mg cm^{-3}) was as low as 0.025 W m^{-1} k^{-1}, which is close to still air (0.023 W m^{-1} k^{-1}), showing a broad prospect in high-temperature insulation. However, the sponge suffers from poor bending performance, and structural damage and fracture will occur under a small bending strain (< 5%). Therefore, these materials can only be used in some thermal insulation places in the form of flat plates, greatly limiting their application field.

To solve the problem of poor bending performance of fiber sponges, Dou et al. obtained SiO_2 nanofiber sponges with good continuity and interwoven cell structure integrating nanofibers with a high aspect ratio and random multidirectional freezing method [95]. The high continuity of the building blocks and cell structures endowed the fiber sponge with good bending and compression properties, which could fully recover to the original position under large compressive and buckling recovery strains (85%). Moreover, the thermal conductivity of the SiO_2 nanofiber sponge was only 0.0223 W m^{-1} K^{-1} with a density of 0.5 mg cm^{-3} (Fig. 13a). In addition, the sponge with a thickness of 1 cm could stabilize the outer layer temperature of the high-temperature pipeline of 700 °C at about 110 °C (Fig. 13b–d), showing good pipeline thermal insulation performance. Since the above-mentioned silica-based sponges exhibit structural collapse and volume shrinkage at extraordinarily high temperatures (> 900 °C); moreover, the effective area of the network assembled by short fibers is very limited, which cannot resist the strong impact and heat flux in practical applications. To solve this problem, Zhang et al. developed anisotropic layered structured ZrO_2–Al_2O_3 nanofiber sponges by stacking flexible nanofiber membranes layer by layer and combining them with an $Al(H_2PO_4)_3$ matrix (Fig. 13e), which exhibited high compressive strength up to 1100 kPa at 90% strain [122]. Moreover, the layered structure and ceramic composition endowed sponges with good compressibility, low thermal conductivity of 0.0322 W m^{-1} K^{-1} (Fig. 13f), and superior thermal insulation properties (Fig. 13g), indicating that they can be served as thermal insulation in extreme conditions.

Air Filtration

Electrospun nanofiber sponges have structural advantages such as large specific surface area, high porosity (> 99%), and controllable thickness, expecting to meet the design requirements of high-performance filter materials with high efficiency, low resistance, and high dust holding capacity [165]. Li et al. prepared electrospun PVDF/HAP nanofiber

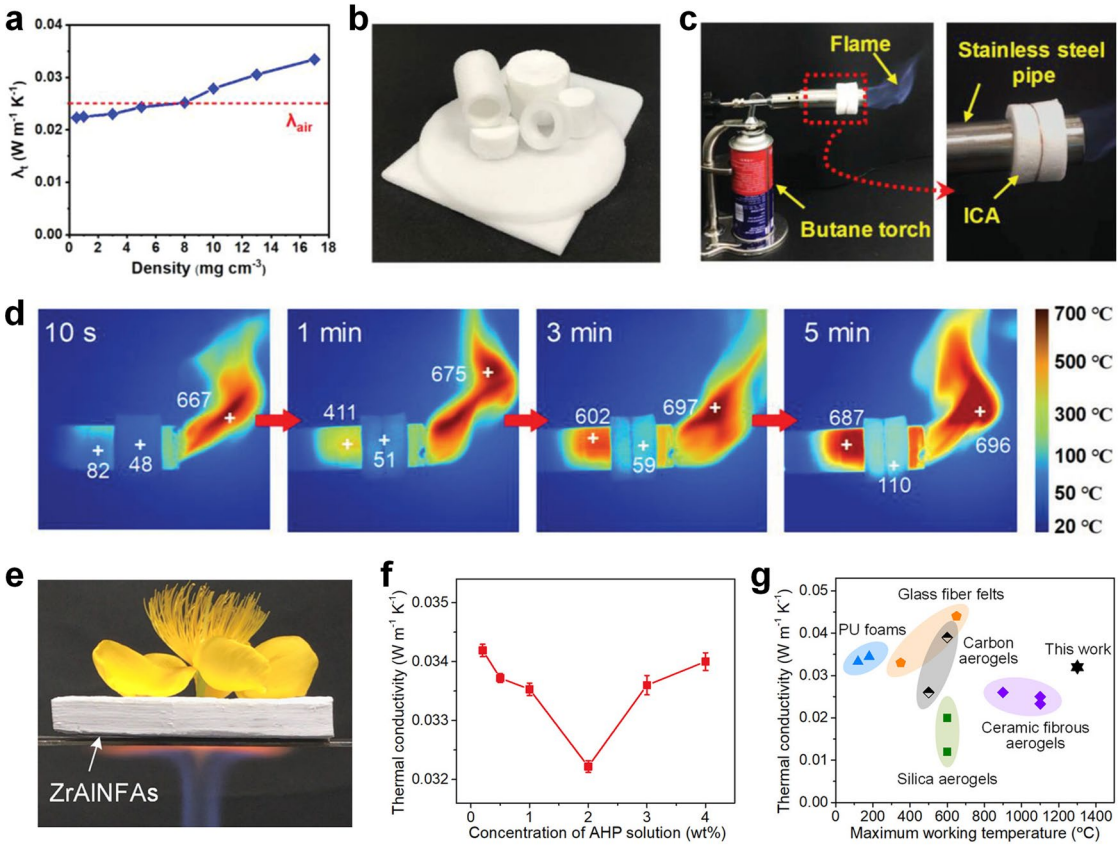

Fig. 13 **a** Thermal conductivity of SiO_2 nanofiber sponges with different densities; **b** optical photos of SiO_2 nanofiber sponges with various shapes; **c** schematic diagram of the thermal insulation testing device of SiO_2 nanofiber sponge; **d** continuous infrared images of butane torch burning within 5 min; Reproduced with permission from Ref. [95]; Copyright 2020, John Wiley and Sons. **e** Demonstration of thermal insulation properties of ZrO_2–Al_2O_3 nanofiber sponges; **f** Thermal conductivity and **g** comparison of comprehensive thermal insulation performance of ZrO_2–Al_2O_3 nanofiber sponges; Reproduced with permission from Ref. [122]; Copyright 2020, American Chemical Society

sponges with wool-like self-crimping structures by adjusting the RH [166]. With the increase of HAP content from 0 to 0.5 wt%, the filtration efficiency of the sponges increased from 84.32% to 99.952%, and the pressure drop increased slightly (from 47 to 50 Pa) (Fig. 14a). By simulating the trapping behavior of sponges with electret and non-electret nanofiber for fine particles, the capture ability of the sponge with electret nanofiber for 0.3 μm particles was significantly enhanced (Fig. 14b). Although the above-mentioned materials have good filtering performance, small thickness leads to low dust holding capacity and short service life. On this basis, Xu et al. prepared electrospun polyimide (PI) sponges with high porosity, which was conducive to the passage of airflow and could intercept particles at high temperatures [167]. However, the low solid content led to small compressive stress (~ 1.4 kPa at 60% strain) and modulus (6.1 kPa) of the sponge, and its structure was easy to collapse when a large number of particles were deposited inside the material or bearing high airflow velocity.

To solve this problem, Li et al. prepared superelastic fiber sponges with high porosity by using PAI as the fiber matrix and bismaleimide as the cross-linking agent, and there were semi-interpenetrating polymer network structures inside the sponge [96]. The PAI-based fibrous sponge exhibited a large Young's modulus (12 kPa) and compressive stress (7.9 kPa). The gradient pore structure was further constructed in the filtration direction of the sponge, and the obtained gradient structured fiber sponge could filter 0.3 μm particles with high efficiency (99.97%), high-temperature stability, and high dust holding capacity of 114 g m^{-2} (Fig. 14c). Besides, gradient fibrous sponges also possessed a good long-term recycling capacity (Fig. 14d). However, it is difficult to intercept tiny particles due to the larger fiber diameter of the sponge and does not have antibacterial and antiviral functions. On this basis, Wang et al. introduced bacterial cellulose (BC) nanofibers into the SiO_2 nanofiber/silane sol dispersion and prepared double network structured nanofiber sponges by combining fiber freeze-drying technology with

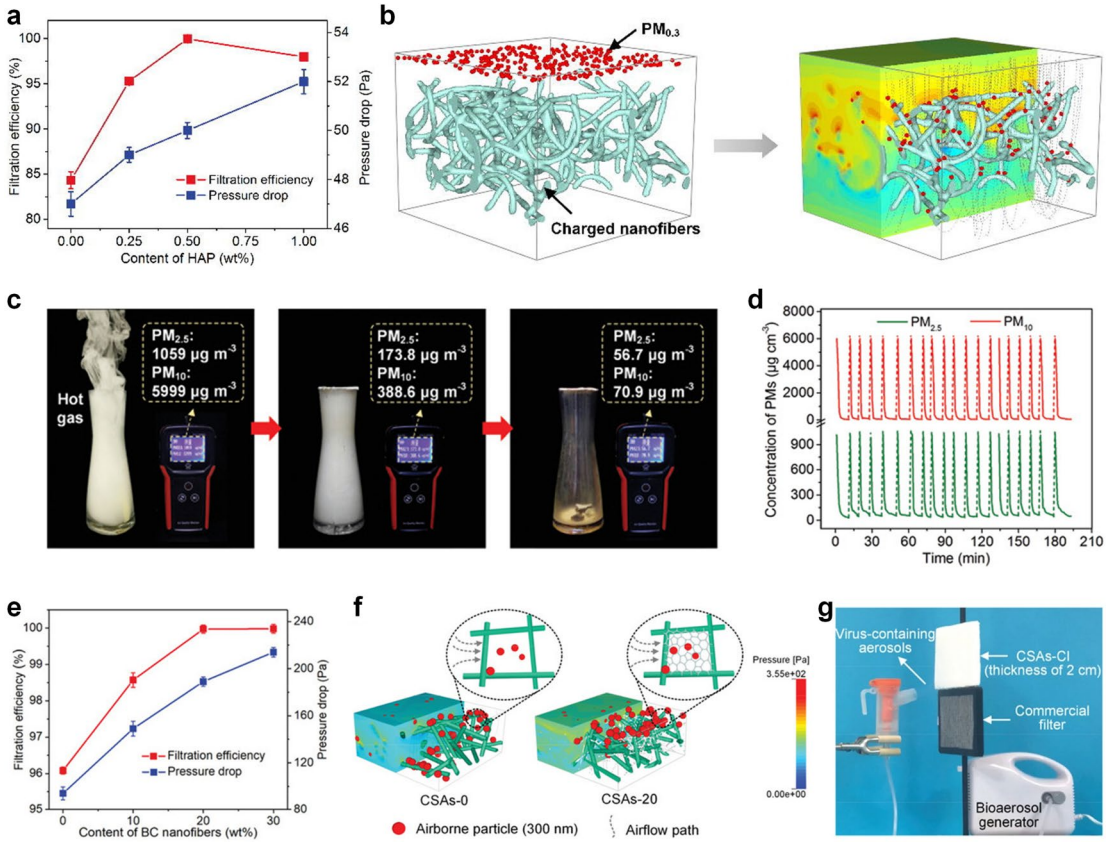

Fig. 14 **a** Filtration efficiency and pressure drop of PVDF fiber sponges with different HAP contents; **b** simulation of filtration process of 0.3 μm particles by charged PVDF nanofiber sponges; Reproduced with permission from Ref. [166]; Copyright 2020, Elsevier. **c** The filtration process of PI fiber sponge to fine particles produced by the combustion of smoke cake; **d** long-term filtration performance of gradient-structured PI nanofiber sponges for $PM_{2.5}$ and PM_{10}; Reproduced with permission from Ref. [96]; Copyright 2020, John Wiley and Sons. **e** Filtration efficiency and pressure drop of SiO_2 fiber sponges on $PM_{0.3}$ with different BC contents; **f** simulation of airflow pressure field during filtration of 0.3 μm particles by fiber sponges with and without BC; **g** filtration performance test of fiber sponge for virus-containing aerosols; reproduced with permission from Ref. [97]; Copyright 2021, John Wiley and Sons

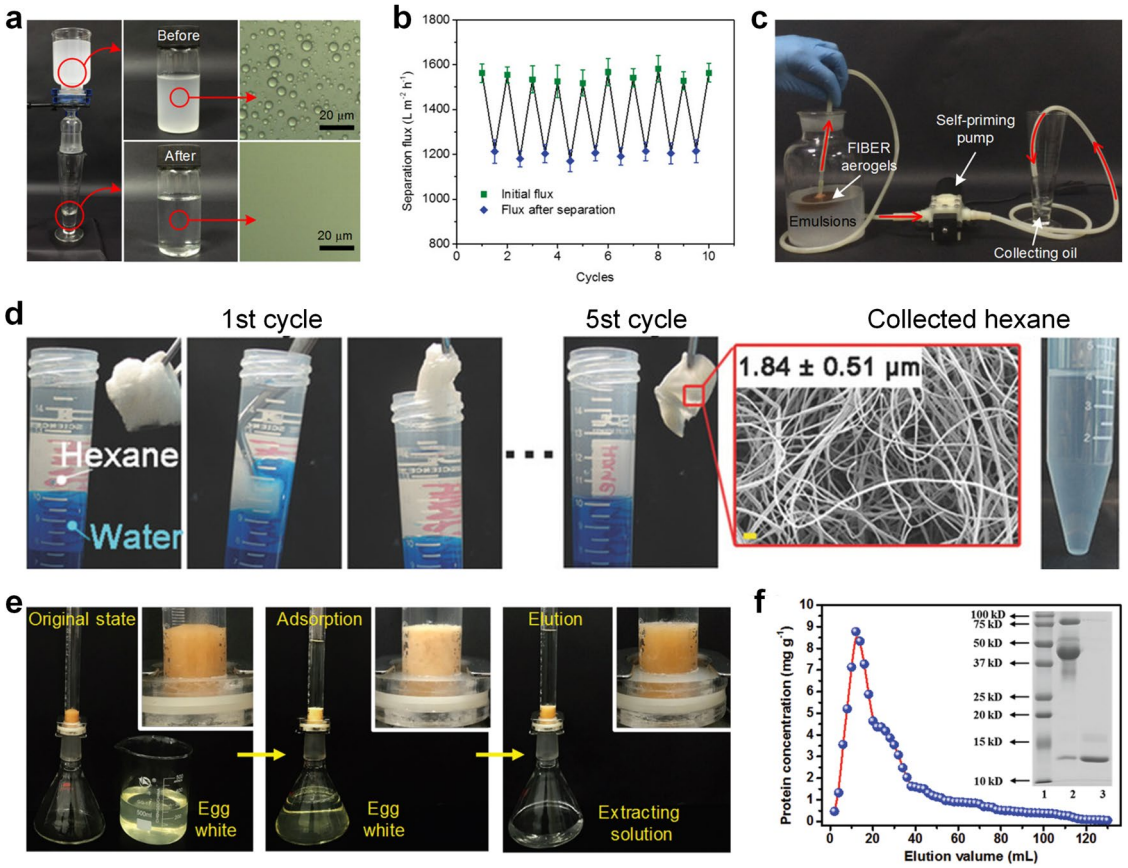

Fig. 15 **a** Separation device of water-in-oil emulsion driven by gravity and optical microscope picture of water and oil after separation; **b** initial fluxes and fluxes after separation during 10 cycles of separation; **c** schematic diagram of oil collecting device continuously extracting pure oil from a water-in-oil emulsion; reproduced with permission from Ref. [32]; Copyright 2015, American Chemical Society. (d) Separation of hexane/water emulsion using PGS/PSU fiber sponge and SEM images of the sponge after five cycles of separation; reproduced with permission from Ref. [171]; Copyright 2017, John Wiley and Sons. **e** Photograph of continuous separation and extraction of lysozyme using carboxylated nanofiber sponge-packed columns; **f** dynamic elution curve of fiber sponge packed column after protein lysozyme extraction; reproduced with permission from Ref. [31]; Copyright 2019, John Wiley and Sons

chlorination treatment [97]. With the increase of BC content, the filtration performance and resistance pressure drop of the sponge gradually increased, which reached 99.97% and 189 Pa when the BC content was 20 wt% (Fig. 14e). By constructing the 3D structural model of the double-network sponge, it could be seen that the secondary BC network inside the sponge could effectively intercept tiny particles (Fig. 14f). In addition, the application of sponge in the field of sterilization and virus-killing air purification was explored, and it was found that sponge could kill 6 logs of Escherichia coli and viruses within 5 min, which is superior to commercial air filter material (Fig. 14g).

Adsorption and Separation

The small pore size, high specific surface area, and good structure adjustability endow porous fiber sponges with high porosity and good pore connectivity, which is conducive to the rapid transport of media [168]. Therefore, they show great application potential in fields of oil–water separation and protein separation [168–170]. Si et al. prepared fibrous sponges using PAN nanofibers and SiO_2 nanofibers as building blocks; meanwhile, cross-linking agent BA-a was in situ introduced into the PAN nanofibers, endowing the sponge with superelasticity through thermal cross-linking [94]. In addition, the low surface energy polybenzoxazine endowed fiber sponges with hydrophobic and lipophilic properties. When the water-in-oil emulsion contacted the sponge surface, oil droplets quickly passed through while water was trapped on the sponge surface, with separating fluxes up to 8100 L m^{-2} h^{-1}. On this basis, SiO_2 nanoparticles were further introduced into the fiber sponge to enhance the hierarchical rough structure, thus the water contact angle of the sponge was up to 162° [32]. When the prepared water-in-oil emulsion was poured into the sponge,

the oil immediately penetrated through the sponge driven by gravity. Meanwhile, the emulsion droplets break upon contact with the sponge, and the water remained on top. The optical micrographs of the collected filtrate showed that no droplets were observed throughout the image, and the separation efficiency exceeded 99.995% (Fig. 15a). In addition, the fiber sponge also had good long-term cycle separation performance (Fig. 15b). By introducing a simple and convenient peristaltic pump, the pure oil was absorbed by the sponge and flowed to the collection cup along the pipeline, realizing the continuous and efficient separation of water-in-oil emulsion (Fig. 15c). Subsequently, Jang et al. prepared core–shell structured poly(glycerol sebacate) (PGS)/PSU fibrous sponges by coaxial electrospinning, following thermal crosslinking endowing the sponge with good elasticity and thermal stability [171]. The presence of the PSU shell endowed the fiber sponge with hydrophobicity and lipophilicity, which effectively separated hexane from water and kept the pore structure and fiber diameter unchanged after five recycling (Fig. 15d).

In the protein separation field, Fu et al. prepared carboxylated nanofiber sponges with honeycomb-like structures by combining the construction of nanofiber sponge with in-situ carboxylation modification, using flexible SiO_2 fiber as a construction unit, PVA as a binder, and citric acid as crosslinker [31]. The hierarchical cellular structure endowed the carboxylated fiber sponge with ultralight properties and superior underwater compression resilience, with plastic deformation of ~ 0% after thousands of underwater compression cycles. Benefiting from connected carboxylated cellular structure, good hydrophilicity, and structural stability, the static and dynamic protein adsorption capacity of the obtained carboxylated fiber sponge reached 2.9×10^3 and 1.7×10^3 mg g^{-1}, respectively; the buffer flux under gravity drove reached 2.17×10^4 L h^{-1} m^{-2}. The comprehensive performance of the sponge was better than previously reported nanofibers and commercial fibrous protein adsorption/separation materials. In addition, the obtained carboxylated nanofibrous sponge could continuously separate lysozyme from egg white solution only under the drive of gravity, showing good practical application prospects (Fig. 15e, f). On this basis, phosphorylated nanofibrous sponges with isotropic structures were prepared by integrating electrospinning, low-temperature induced phase separation regulation, and blending phosphorylation modification techniques [172]. The obtained phosphorylated fibrous sponges exhibited significantly improved static (3.3×10^3 mg g^{-1}) and dynamic (1.8×10^3 mg g^{-1}) protein adsorption performance, and the buffer flux under gravity-driven reached 1.5×10^4 L h^{-1} m^{-2}.

Tissue Engineering

The fibers diameter of the electrospun nanofiber sponge is generally between tens of nanometers and several micrometers, which is similar to the nanofiber structure of the ECM, so it is conducive to cell adhesion, proliferation, migration, and differentiation [173]. Moreover, 3D interconnected spatial structures make it suitable for nutrient transport and cell/vascular growth, showing wide applications in tissue engineering and regenerative medicine [24, 63, 174]. Wang et al. constructed 3D SiO_2 nanofiber/chitosan (SiO_2 NF/CS) elastic scaffold through homogenous dispersion, in-situ crosslinking, and freeze-drying [92]. Then, the biocompatibility of SiO_2 NF/CS scaffolds in vitro and the effect on the differentiation behavior of hMSCs were examined (Fig. 16a). Furthermore, bone defect models with different shapes were constructed in the rabbit mandible, and the results confirmed that the good resilience of the SiO_2 NF/CS scaffold made it adaptive to bone defects in vivo and achieved minimally invasive surgery (Fig. 16b, c). On this basis, the scaffolds were implanted into skull defects of rats, and the results of skull repair showed that the implantation of SiO_2 NF/CS scaffolds could increase the bone volume fraction (30–40%) and bone mineral density of new bone (Fig. 16d–f). This enhanced the expression of osteogenic-related and vascular-related proteins, thus promoting the formation of bone and blood vessels. To solve the problem that single structured scaffolds cannot meet the diversity of bone-soft tissue interfaces, gradient SiO_2 NF/CS scaffolds with gradient distribution in morphology, structure, and mineralization properties were prepared. The gradient scaffold could induce the bidirectional differentiation of hMSCs into osteogenic and cartilage cells, showing potential application value in the repair of subchondral bone defects. However, due to the low biomineralization activity of SiO_2 nanofibers, it is difficult to meet the efficient repair of osteoporotic bone defects. 3D SiO_2–CaO nanofibers/CS scaffolds were prepared by introducing CaO into the SiO_2 molecular network, and the elasticity of the scaffolds made them suitable for various shapes of defects, which is convenient for the use of minimally invasive surgery [175].

Recently, Mo et al. prepared 3D bionic nerve conduits through nanofiber dispersion, freeze-drying, and cross-linking by using tussah SF/(poly(L-lactic acid-*co*-caprolactone)) (PLCL)/GO nanofibers as raw materials [176]. Further in vitro studies indicated that the neural scaffold could provide an effective guiding interface for neuronal cell growth, and the nerve conduits were almost completely degraded within 12 weeks. These results suggest that the 3D hierarchical nerve conduits with fascicular structures exhibited huge advantages in peripheral nerve repair. Subsequently, 3D PLCL/SF scaffolds (3DS) and 3D HA-crosslinked scaffolds (3DHAS) were successfully prepared by dynamic

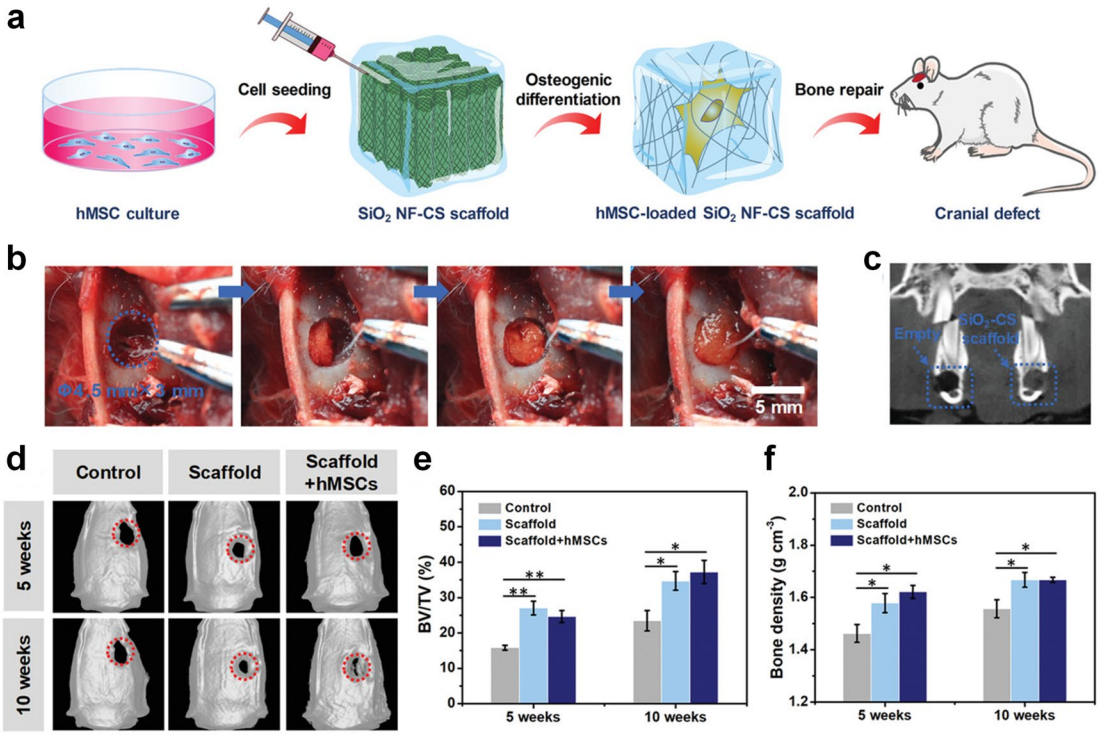

Fig. 16 **a** Schematic diagram of experimental design of in vitro culture and in vivo transplantation of hMSCs in SiO_2 NF/CS scaffolds; **b** photos of SiO_2 NF/CS scaffolds implanted into round mandibular defects in rabbits; **c** 2D computed tomography (CT) images of bone defects showed the scaffold was in close contact with the host bone; **d** 3D reconstructed CT images of rat skull defect at 5 and 10 weeks after surgery; **e** bone volume fraction and **f** bone mineral density at 5 and 10 weeks postoperatively; reproduced with permission from Ref. [92]; Copyright 2019, John Wiley and Sons

liquid bath collection, in-situ gas foaming, and freeze-drying [177]. Compared with 3DS, 3DHAS showed better chondrocyte proliferative capacity and supported the chondrogenic phenotype in vitro. Histological analysis of the transplanted cytoskeleton structures after implantation for 8 weeks showed that both 3DS and 3DHAS formed cartilage-like tissue, and the cartilage lacunae formed in the 3DHAS were more mature. After implantation for up to 12 weeks in a rabbit articular cartilage defect model, the 3DHAS showed better scaffold repair ability.

Conclusions

In the past few decades, 3D electrospun fibrous materials have found broad application prospects in the fields of environmental protection, safety protection, tissue engineering, etc. owing to their unique 3D spatial structure, large specific surface area, high porosity, and lightweight features. In recent years, the construction of electrospun nanofiber sponges mainly includes 3D reconstruction and direct electrospinning. In the 3D reconstruction of electrospun fiber membranes, the successful fabrications of fiber sponges have been achieved by embedding in hydrogels, 3D printing, gas-foaming, or freeze-drying. In direct electrospinning, researchers have obtained 3D porous fiber materials with different morphology and structure employing layer-by-layer stacking, liquid-assisted collection, 3D template collection, particle leaching, and humidity field regulation method. These methods have successfully achieved the effective preparation of 3D fiber materials and the specific applications in the fields such as sound absorption, warmth retention, thermal insulation, air filtration, adsorption/separation, and tissue engineering, providing a good start for subsequent application research. Therefore, the recent research progress of electrospun fiber sponges from their principle, fabrication, and functional applications was reviewed.

Outlooks

Although breakthroughs have been made in the preparation of 3D fibrous materials, there are still great challenges in preparation and practical applications, which need to be further solved with greater efforts in the future. For example, although fiber sponges with certain mechanical strength were prepared by embedding fibers in hydrogels, they are not suitable for water-soluble polymers, and their

application fields are limited; 3D printing and gas-foaming methods usually require freeze-drying to fix the shape of fibrous sponges; Although the freeze-drying method could fabricate fiber sponges with controllable structure and morphology, it takes a long time and consumes a lot of energy, which increases the difficulty of macro-scale preparation of sponges. Moreover, the fibers in the sponge prepared by the layer-by-layer stacking method are still distributed in layers, which cannot achieve real 3D connectivity; The shape and size of fiber sponges prepared by liquid-assisted collection and 3D template collection method are poorly controllable and usually need further treatment; The pore size of the fiber sponge prepared by the particle leaching method has a limited adjustable range, and the particles are easy to remain; The preparation by humidity field regulation method is relatively simple, but this method still suffers from the single and uncontrollable internal structure of obtained fiber sponges. Besides, most of the current research on the preparation and application of electrospun fiber sponges is at the level of laboratory research, and there is an urgent need for large-scale and high-quality production of fiber sponges.

Based on the above-mentioned preliminary research foundation of nanofiber sponges, it can be expected that future research work on electrospun materials will strive to achieve the following breakthroughs: (1) Improve the structural stability of fiber sponges. The refinement of fiber improves the functionality of the material but reduces the mechanical properties of the material, so it is necessary to further improve the structural stability of the fiber sponges. The mechanical strengthening of fiber sponges can start from electrospun raw materials, giving preference to polymers with good mechanical properties, and deeply studying the influence of spinning solution and processing parameters on the structure of fiber sponges. Subsequently, the stress failure processes (including compression, tension, and shear) of fiber sponges are analyzed, and the results are used for feedback on the microstructure design, thus further improving the mechanical properties of the fiber sponge. (2) Further broaden the application field of fibrous sponges. Fiber sponges usually need to be used in combination with supporting substrates in some fields such as filtration and separation, high-temperature thermal insulation, etc., but the material is easily damaged during the compounding process. Therefore, low-damage compound technologies of 3D fiber materials need to be developed to achieve the multifunctionalization of materials, which can further expand the application field of nanofiber materials. Besides, by introducing functional substances (such as nanoparticles, nanosheets, etc.) into nanofiber sponges, the materials can be endowed with additional functions, such as magnetism, light absorption, and antibacterial/antiviral properties. (3) Achieve mass production of 3D fiber materials. Due to the limitations of the production process and equipment, most of the 3D fiber sponges are still at the laboratory level, which is difficult to meet the size and output required for practical application. Therefore, it is necessary to develop production equipment by integrating the specific structural characteristics of fiber sponges, then achieving the uniform and stable enlarged preparation of 3D fiber sponges.

Acknowledgements This work was supported by the Ministry of Science and Technology of China (2021YFE0105100), the Natural Science Foundation of China (51873031 and 52103050), the Science and Technology Commission of Shanghai Municipality (21ZR1402600 and 21ZR1401800), and the Fundamental Research Funds for the Central Universities (CUSF-DH-D-2020040).

Declarations

Conflict of Interest The authors declare no competing financial interest.

References

1. Ma W, Zhang Y, Pan S, Cheng Y, Shao Z, Xiang H, Chen G, Zhu L, Weng W, Bai H, Zhu M. Smart fibers for energy conversion and storage. *Chem Soc Rev* **2021**;*50*:7009.
2. Chang H, Luo J, Gulgunje PV, Kumar S. Structural and functional fibers. *Annu Rev Mater Res* **2017**;*47*:331.
3. Priyanka P, Dixit A, Mali HS. High strength kevlar fiber reinforced advanced textile composites. *Iran Polym J* **2019**;*28*:621.
4. Shi Q, Sun J, Hou C, Li Y, Zhang Q, Wang H. Advanced functional fiber and smart textile. *Adv Fiber Mater* **2019**;*1*:3.
5. Baye B, Tesfaye T. The new generation fibers: a review of high performance and specialty fibers. *Polym Bull* **2021**. https://doi.org/10.1007/s00289-021-03966-6 .
6. Saito N, Aoki K, Usui Y, Shimizu M, Hara K, Narita N, Ogihara N, Nakamura K, Ishigaki N, Kato H, Haniu H, Taruta S, Kim YA, Endo M. Application of carbon fibers to biomaterials: a new era of nano-level control of carbon fibers after 30-years of development. *Chem Soc Rev* **2011**;*40*:3824.
7. Joshi M, Butola BS, Saha K. Advances in topical drug delivery system: micro to nanofibrous structures. *J Nanosci Nanotechnol* **2014**;*14*:853.
8. Kenry, Lim CT. Nanofiber technology: current status and emerging developments. *Prog Polym Sci* **2017**;*70*:1.
9. Kim BS, Kim IS. Recent nanofiber technologies. *Polym Rev* **2011**;*51*:235.
10. Zhou X, Wang Y, Gong C, Liu B, Wei G. Production, structural design, functional control, and broad applications of carbon nanofiber-based nanomaterials: a comprehensive review. *Chem Eng J* **2020**;*402*:126189.
11. Matsumoto H, Tanioka A. Functionality in electrospun nanofibrous membranes based on fiber's size, surface area, and molecular orientation. *Membranes* **2011**;*1*:249.
12. Toriello M, Afsari M, Shon HK, Tijing LD. Progress on the fabrication and application of electrospun nanofiber composites. *Membranes* **2020**;*10*:204.
13. Stout DA. Recent advancements in carbon nanofiber and carbon nanotube applications in drug delivery and tissue engineering. *Curr Pharm Design* **2015**;*21*:2037.
14. Parveen S, Rana S, Fangueiro R. A review on nanomaterial dispersion, microstructure, and mechanical properties of carbon

nanotube and nanofiber reinforced cementitious composites. *J Nanomater* **2013**;*2013*:710175.
15. Wang X, Ding B, Sun G, Wang M, Yu J. Electro-spinning/netting: a strategy for the fabrication of three-dimensional polymer nano-fiber/nets. *Prog Mater Sci* **2013**;*58*:1173.
16. Garg T, Rath G, Goyal AK. Biomaterials-based nanofiber scaffold: targeted and controlled carrier for cell and drug delivery. *J Drug Target* **2015**;*23*:202.
17. Sundaramurthi D, Krishnan UM, Sethuraman S. Electrospun nanofibers as scaffolds for skin tissue engineering. *Polym Rev* **2014**;*54*:348.
18. Xue J, Wu T, Dai Y, Xia Y. Electrospinning and electrospun nanofibers: methods, materials, and applications. *Chem Rev* **2019**;*119*:5298.
19. Liao X, Dulle M, de Souza e Silva JM, Wehrspohn RB, Agarwal S, Foerster S, Hou H, Smith P, Greiner A. High strength in combination with high toughness in robust and sustainable polymeric materials. *Science* **2019**;*366*:1376.
20. Xue J, Xie J, Liu W, Xia Y. Electrospun nanofibers: new concepts, materials, and applications. *Accounts Chem Res* **1976**;*2017*:50.
21. Inagaki M, Yang Y, Kang F. Carbon nanofibers prepared via electrospinning. *Adv Mater* **2012**;*24*:2547.
22. Fadil F, Affandi NDN, Misnon MI, Bonnia NN, Harun AM, Alam MK. Review on electrospun nanofiber-applied products. *Polymers* **2021**;*13*:2087.
23. Sun B, Long YZ, Zhang HD, Li MM, Duvail JL, Jiang XY, Yin HL. Advances in three-dimensional nanofibrous macrostructures via electrospinning. *Prog Polym Sci* **2014**;*39*:862.
24. Chen Y, Dong X, Shafiq M, Myles G, Radacsi N, Mo X. Recent advancements on three-dimensional electrospun nanofiber scaffolds for tissue engineering. *Adv Fiber Mater* **2022**. https://doi.org/10.1007/s42765-022-00170-7 .
25. Xu T, Ding Y, Liang Z, Sun H, Zheng F, Zhu Z, Zhao Y, Fong H. Three-dimensional monolithic porous structures assembled from fragmented electrospun nanofiber mats/membranes: methods, properties, and applications. *Prog Mater Sci* **2020**;*112*:100656.
26. Han S, Nie K, Li J, Sun Q, Wang X, Li X, Li Q. 3D electrospun nanofiber-based scaffolds: from preparations and properties to tissue regeneration applications. *Stem Cells Int* **2021**;*2021*:8790143.
27. Cao LT, Fu QX, Si Y, Ding B, Yu JY. Porous materials for sound absorption. *Compos Commun* **2018**;*10*:25.
28. Cao L, Shan H, Zong D, Yu X, Yin X, Si Y, Yu J, Ding B. Fire-resistant and hierarchically structured elastic ceramic nanofibrous aerogels for efficient low-frequency noise reduction. *Nano Lett* **2022**;*22*:1609.
29. Si Y, Wang X, Dou L, Yu J, Ding B. Ultralight and fire-resistant ceramic nanofibrous aerogels with temperature-invariant superelasticity. *Sci Adv* **2018**;*4*:eaas8925.
30. Cheng X, Liu Y, Si Y, Yu J, Ding B. Direct synthesis of highly stretchable ceramic nanofibrous aerogels via 3D reaction electrospinning. *Nat Commun* **2022**;*13*:2637.
31. Fu Q, Si Y, Duan C, Yan Z, Liu L, Yu J, Ding B. Highly carboxylated, cellular structured, and underwater superelastic nanofibrous aerogels for efficient protein separation. *Adv Funct Mater* **2019**;*29*:1808234.
32. Si Y, Fu Q, Wang X, Zhu J, Yu J, Sun G, Ding B. Superelastic and superhydrophobic nanofiber-assembled cellular aerogels for effective separation of oil/water emulsions. *ACS Nano* **2015**;*9*:3791.
33. Huang C, Soenen SJ, Rejman J, Lucas B, Braeckmans K, Demeester J, De Smedt SC. Stimuli-responsive electrospun fibers and their applications. *Chem Soc Rev* **2011**;*40*:2417.
34. Zhang B, Kang F, Tarascon J, Kim J. Recent advances in electrospun carbon nanofibers and their application in electrochemical energy storage. *Prog Mater Sci* **2016**;*76*:319.
35. Luo CJ, Stoyanov SD, Stride E, Pelan E, Edirisinghe M. Electrospinning *versus* fibre production methods: from specifics to technological convergence. *Chem Soc Rev* **2012**;*41*:4708.
36. Li D, Xia YN. Electrospinning of nanofibers: reinventing the wheel? *Adv Mater* **2004**;*16*:1151.
37. Taylor GI. Disintegration of water drops in an electric field. *Proc R Soc Lond A* **1964**;*280*:383.
38. Reneker DH, Yarin AL. Electrospinning jets and polymer nanofibers. *Polymer* **2008**;*49*:2387.
39. Reneker DH, Yarin A, Zussman E, Koombhongse S, Kataphinan W. Nanofiber manufacturing: toward better process control. In: Reneker DH, Fong H, editors. Polymeric nanofibers. Washington: American Chemical Society; **2006**. p. 7–20.
40. Shin YM, Hohman MM, Brenner MP, Rutledge GC. Experimental characterization of electrospinning: the electrically forced jet and instabilities. *Polymer* **2001**;*42*:9955.
41. Agarwal S, Greiner A, Wendorff JH. Functional materials by electrospinning of polymers. *Prog Polym Sci* **2013**;*38*:963.
42. Yoon J, Yang H, Lee B, Yu W. Recent progress in coaxial electrospinning: new parameters, various structures, and wide applications. *Adv Mater* **2018**;*30*:1704765.
43. Rahmati M, Mills DK, Urbanska AM, Saeb MR, Venugopal JR, Ramakrishna S, Mozafari M. Electrospinning for tissue engineering applications. *Prog Mater Sci* **2021**;*117*:100721.
44. Shi S, Si Y, Han Y, Wu T, Iqbal MI, Fei B, Li RKY, Hu J, Qu J. Recent progress in protective membranes fabricated via electrospinning: advanced materials, biomimetic structures, and functional applications. *Adv Mater* **2022**;*34*:2107938.
45. Taylor GI. Electrically driven jets. *Proc Roy Soc Lond A* **1969**;*313*:453.
46. He JH, Wu Y, Zuo WW. Critical length of straight jet in electrospinning. *Polymer* **2005**;*46*:12637.
47. Lin JY, Ding B, Yu JY, Wu GC, Yang JM, Sun G. Effect of porous structure of electrospun fibers on their specific surface area: theoretical analysis and experimental verification. *Int J Nonlinear Sci Num* **2010**;*11*:523.
48. Lin JY, Cai Y, Wang XF, Ding B, Yu JY, Wang MR. Fabrication of biomimetic superhydrophobic surfaces inspired by lotus leaf and silver ragwort leaf. *Nanoscale* **2011**;*3*:1258.
49. Fashandi H, Karimi M. Pore formation in polystyrene fiber by superimposing temperature and relative humidity of electrospinning atmosphere. *Polymer* **2012**;*53*:5832.
50. Chen X, Xu Y, Zhang W, Xu K, Ke Q, Jin X, Huang C. Online fabrication of ultralight, three-dimensional, and structurally stable ultrafine fibre assemblies with a double-porous feature. *Nanoscale* **2019**;*11*:8185.
51. Lin J, Ding B, Yu J, Hsieh Y. Direct fabrication of highly nanoporous polystyrene fibers via electrospinning. *ACS Appl Mater Interfaces* **2010**;*2*:521.
52. Lu P, Xia Y. Maneuvering the internal porosity and surface morphology of electrospun polystyrene yarns by controlling the solvent and relative humidity. *Langmuir* **2013**;*29*:7070.
53. Cao L, Si Y, Yin X, Yu J, Ding B. Ultralight and resilient electrospun fiber sponge with a lamellar corrugated microstructure for effective low-frequency sound absorption. *ACS Appl Mater Interfaces* **2019**;*11*:35333.
54. Zhang C, Yu S. Nanoparticles meet electrospinning: recent advances and future prospects. *Chem Soc Rev* **2014**;*43*:4423.
55. Dias JR, Granja PL, Bartolo PJ. Advances in electrospun skin substitutes. *Prog Mater Sci* **2016**;*84*:314.
56. Cooper CJ, Mohanty AK, Misra M. Electrospinning process and structure relationship of biobased poly(butylene succinate) for nanoporous fibers. *ACS Omega* **2018**;*3*:5547.
57. Fu Q, Duan C, Yan Z, Li Y, Si Y, Liu L, Yu J, Ding B. Nanofiber-based hydrogels: controllable synthesis and multifunctional applications. *Macromol Rapid Comm* **2018**;*39*:1800058.

58. Lu X, Si Y, Zhang S, Yu J, Ding B. In situ synthesis of mechanically robust, transparent nanofiber-reinforced hydrogels for highly sensitive multiple sensing. *Adv Funct Mater* **2021**;*31*:2103117.
59. Xu W, Ma J, Jabbari E. Material properties and osteogenic differentiation of marrow stromal cells on fiber-reinforced laminated hydrogel nanocomposites. *Acta Biomater* **1992**;*2010*:6.
60. An D, Ji Y, Chiu A, Lu YC, Song W, Zhai L, Qi L, Luo D, Ma M. Developing robust, hydrogel-based, nanofiber-enabled encapsulation devices (NEEDs) for cell therapies. *Biomaterials* **2015**;*37*:40.
61. Si Y, Wang L, Wang X, Tang N, Yu J, Ding B. Ultrahigh-water-content, superelastic, and shape-memory nanofiber-assembled hydrogels exhibiting pressure-responsive conductivity. *Adv Mater* **2017**;*29*:1700339.
62. Coburn J, Gibson M, Bandalini PA, Laird C, Mao HQ, Moroni L, Seliktar D, Elisseeff J. Biomimetics of the extracellular matrix: an integrated three-dimensional fiber-hydrogel composite for cartilage tissue engineering. *Smart Struct Syst* **2011**;*7*:213.
63. Chen Y, Shafiq M, Liu M, Morsi Y, Mo X. Advanced fabrication for electrospun three-dimensional nanofiber aerogels and scaffolds. *Bioact Mater* **2020**;*5*:963.
64. Chen W, Xu Y, Liu Y, Wang Z, Li Y, Jiang G, Mo X, Zhou G. Three-dimensional printed electrospun fiber-based scaffold for cartilage regeneration. *Mater Design* **2019**;*179*:107886.
65. Chen W, Xu Y, Li Y, Jia L, Mo X, Jiang G, Zhou G. 3D printing electrospinning fiber-reinforced decellularized extracellular matrix for cartilage regeneration. *Chem Eng J* **2019**;*382*:122986.
66. Lee S, Nowicki M, Harris B, Zhang LG. Fabrication of a highly aligned neural scaffold via a table top stereolithography 3D printing and electrospinning. *Tissue Eng A* **2017**;*23*:491.
67. Yu Y, Hua S, Yang M, Fu Z, Teng S, Niu K, Zhao Q, Yi C. Fabrication and characterization of electrospinning/3D printing bone tissue engineering scaffold. *RSC Adv* **2016**;*6*:110557.
68. Rampichová M, Kuželová EK, Filová E, Chvojka J, Šafk J, Pelcl M, Daňková J, Prosecká E, Buzgo M, Plencner M, Lukáš D, Amler E. Composite 3D printed scaffold with structured electrospun nanofibers promotes chondrocyte adhesion and infiltration. *Cell Adhes Migr* **2018**;*12*:271.
69. Yuan H, Zhou Q, Li B, Bao M, Lou X, Zhang Y. Direct printing of patterned three-dimensional ultrafine fibrous scaffolds by stable jet electrospinning for cellular ingrowth. *Biofabrication* **2015**;*7*:045004.
70. Yi B, Zhang H, Yu Z, Yuan H, Wang X, Zhang Y. Fabrication of high performance silk fibroin fibers *via* stable jet electrospinning for potential use in anisotropic tissue regeneration. *J Mater Chem B* **2018**;*6*:3934.
71. Jin X, Al-Qatatsheh A, Subhani K, Salim NV. Biomimetic and flexible 3D carbon nanofiber networks with fire-resistant and high oil-sorption capabilities. *Chem Eng J* **2021**;*412*:128635.
72. Zhao P, Cao MY, Gu HB, Gao Q, Xia N, He Y, Fu JZ. Research on the electrospun foaming process to fabricate three-dimensional tissue engineering scaffolds. *J Appl Polym Sci* **2018**;*135*:46898.
73. Chen YJ, Jia ZH, Shafiq M, Xie XR, Xiao XH, Castro R, Rodrigues J, Wu JL, Zhou GD, Mo XM. Gas foaming of electrospun poly(L-lactide-co-caprolactone)/silk fibroin nanofiber scaffolds to promote cellular infiltration and tissue regeneration. *Colloid Surf B* **2021**;*201*:111637.
74. Zhang K, Bai X, Yuan Z, Cao X, Jiao X, Li Y, Qin Y, Wen Y, Zhang X. Layered nanofiber sponge with an improved capacity for promoting blood coagulation and wound healing. *Biomaterials* **2019**;*204*:70.
75. Rao F, Yuan Z, Li M, Yu F, Fang X, Jiang B, Wen Y, Zhang P. Expanded 3D nanofibre sponge scaffolds by gas-foaming technique enhance peripheral nerve regeneration. *Artif Cell Nanomed Biotechnol* **2019**;*47*:491.
76. Kim SE, Tiwari AP. Three dimensional polycaprolactone/cellulose scaffold containing calcium-based particles: a new platform for bone regeneration. *Carbohyd Polym* **2020**;*250*:116880.
77. Joshi MK, Pant HR, Tiwari AP, Kim HJ, Park CH, Kim CS. Multi-layered macroporous three-dimensional nanofibrous scaffold via a novel gas foaming technique. *Chem Eng J* **2015**;*275*:79.
78. Jiang J, Carlson MA, Teusink MJ, Wang H, MacEwan MR, Xie J. Expanding two-dimensional electrospun nanofiber membranes in the third dimension by a modified gas-foaming technique. *ACS Biomater Sci Eng* **2015**;*1*:991.
79. Jiang J, Li Z, Wang H, Wang Y, Carlson MA, Teusink MJ, MacEwan MR, Gu L, Xie J. Expanded 3D nanofiber scaffolds: cell penetration, neovascularization, and host response. *Adv Healthc Mater* **2016**;*5*:2993.
80. Jia ZH, Liu Y, Wang YY, Peng SY, Jia P, Zhang W, Tan XY. Gas-foaming three-dimensional electrospun nanofiber scaffold improved three-dimensional cartilage regeneration. *Mater Res Express* **2021**;*8*:085403.
81. Karki HP, Kafle L, Ojha DP, Song JH, Kim HJ. Three-dimensional nanoporous polyacrylonitrile-based carbon scaffold for effective separation of oil from oil/water emulsion. *Polymer* **2018**;*153*:597.
82. Karki HP, Kafle L, Kim HJ. Modification of 3D polyacrylonitrile composite fiber for potential oil-water mixture separation. *Sep Purif Technol* **2019**;*229*:115840.
83. Yuan ZP, Li YS, Zhao D, Zhang KX, Wang F, Wang CT, Wen YQ. High efficiency 3D nanofiber sponge for bilirubin removal used in hemoperfusion. *Colloid Surf B* **2018**;*172*:161.
84. Gao Q, Gu HB, Zhao P, Zhang CM, Cao MY, Fu J, He Y. Fabrication of electrospun nanofibrous scaffolds with 3D controllable geometric shapes. *Mater Des* **2018**;*157*:159.
85. Jing X, Li H, Mi H, Liu Y, Tan Y. Fabrication of fluffy shish-kebab structured nanofibers by electrospinning, CO_2 escaping foaming and controlled crystallization for biomimetic tissue engineering scaffolds. *Chem Eng J* **2019**;*372*:785.
86. Jiang J, Chen S, Wang H, Carlson MA, Gombart AF, Xie J. CO_2-expanded nanofiber scaffolds maintain activity of encapsulated bioactive materials and promote cellular infiltration and positive host response. *Acta Biomater* **2018**;*68*:237.
87. Dong X, Cao L, Si Y, Ding B, Deng H. Cellular structured CNTs@SiO_2 nanofibrous aerogels with vertically aligned vessels for salt-resistant solar desalination. *Adv Mater* **2020**;*32*:1908269.
88. Zhang M, Wang Y, Zhang Y, Song J, Si Y, Yan J, Ma C, Liu Y, Yu J, Ding B. Conductive and elastic TiO_2 nanofibrous aerogels: a new concept toward self-supported electrocatalysts with superior activity and durability. *Angew Chem Int Ed* **2020**;*59*:2.
89. Zhang M, Zhang L, Huang S, Wang Y, Si Y, Ma C, Zhang P, Liu Y, Yu J, Ding B. 2D gallium molybdenum selenide grown on a hollow carbon nanofibrous aerogel for high-efficiency electroreduction of nitrogen: optimized basal plane activity *via* selenium vacancy modulation. *Appl Catal B-Environ* **2021**;*292*:120175.
90. Liao Y, Song J, Si Y, Yu J, Ding B. Superelastic and photothermal RGO/Zr-doped TiO_2 nanofibrous aerogels enable the rapid decomposition of chemical warfare agents. *Nano Lett* **2022**;*22*:4368.
91. Zhang F, Si Y, Yu J, Ding B. Sub-nanoporous engineered fibrous aerogel molecular sieves with nanogating channels for reversible molecular separation. *Small* **2022**;*18*:2202173.
92. Wang L, Qiu Y, Lv H, Si Y, Liu L, Zhang Q, Cao J, Yu J, Li X, Ding B. 3D superelastic scaffolds constructed from flexible inorganic nanofibers with self-fitting capability and tailorable gradient for bone regeneration. *Adv Funct Mater* **2019**;*29*:1901407.

93. Dong X, Si Y, Chen C, Ding B, Deng H. Reed leaves inspired silica nanofibrous aerogels with parallel-arranged vessels for salt-resistant solar desalination. *ACS Nano* **2021**;*15*:12256.
94. Si Y, Yu J, Tang X, Ge J, Ding B. Ultralight nanofibre-assembled cellular aerogels with superelasticity and multifunctionality. *Nat Commun* **2014**;*5*:5802.
95. Dou L, Zhang X, Shan H, Cheng X, Si Y, Yu J, Ding B. Interweaved cellular structured ceramic nanofibrous aerogels with superior bendability and compressibility. *Adv Funct Mater* **2020**;*30*:2005928.
96. Li Y, Cao L, Yin X, Si Y, Yu J, Ding B. Semi-interpenetrating polymer network biomimetic structure enables superelastic and thermostable nanofibrous aerogels for cascade filtration of $PM_{2.5}$. *Adv Funct Mater* **2020**;*30*:1910426.
97. Wang F, Si Y, Yu J, Ding B. Tailoring nanonets-engineered superflexible nanofibrous aerogels with hierarchical cage-like architecture enables renewable antimicrobial air filtration. *Adv Funct Mater* **2021**;*31*:2107223.
98. Wang F, Dou L, Dai J, Li Y, Huang L, Si Y, Yu J, Ding B. In situ synthesis of biomimetic silica nanofibrous aerogels with temperature-invariant superelasticity over one million compressions. *Angew Chem Int Ed* **2020**;*59*:8285.
99. Cao L, Si Y, Wu Y, Wang X, Yu J, Ding B. Ultralight, superelastic and bendable lashing-structured nanofibrous aerogels for effective sound absorption. *Nanoscale* **2019**;*11*:2289.
100. Wu H, Cai H, Zhang S, Yu J, Ding B. Ultralight, superelastic, and washable nanofibrous sponges with rigid-flexible coupling architecture enable reusable warmth retention. *Nano Lett* **2022**;*22*:830.
101. Cao L, Yu X, Yin X, Si Y, Yu J, Ding B. Hierarchically maze-like structured nanofiber aerogels for effective low-frequency sound absorption. *J Colloid Interf Sci* **2021**;*597*:21.
102. Dou L, Zhang X, Cheng X, Ma Z, Wang X, Si Y, Yu J, Ding B. Hierarchical cellular structured ceramic nanofibrous aerogels with temperature-invariant superelasticity for thermal insulation. *ACS Appl Mater Interfaces* **2019**;*11*:29056.
103. Liao Y, Yang F, Si Y, Yu J, Ding B. Nanoflake-engineered zirconic fibrous aerogels with parallel-arrayed conduits for fast nerve agent degradation. *Nano Lett* **2021**;*21*:8839.
104. Wang F, Dai J, Huang L, Si Y, Yu J, Ding B. Biomimetic and superelastic silica nanofibrous aerogels with rechargeable bactericidal function for antifouling water disinfection. *ACS Nano* **2020**;*14*:8975.
105. Zhang M, Dai J, Huang S, Fang D, Liu Y, Yu J, Ding B, Greiner A. Pt/TiO_{2-x} nanofibrous aerogel for effective nitrogen reduction: a simple strategy for simultaneous Pt formation and TiO_{2-x} vacancy engineering. *Chin Chem Lett* **2022**;*33*:1001.
106. Si Y, Wang X, Yan C, Yang L, Yu J, Ding B. Ultralight biomass-derived carbonaceous nanofibrous aerogels with superelasticity and high pressure-sensitivity. *Adv Mater* **2016**;*28*:9512.
107. Zong D, Cao L, Yin X, Si Y, Zhang S, Yu J, Ding B. Flexible ceramic nanofibrous sponges with hierarchically entangled graphene networks enable noise absorption. *Nat Commun* **2021**;*12*:6599.
108. Ziai Y, Petronella F, Rinoldi C, Nakielski P, Zakrzewska A, Kowalewski TA, Augustyniak W, Li X, Calogero A, Sabala I, Ding B, De Sio L, Pierini F. Chameleon-inspired multifunctional plasmonic nanoplatforms for biosensing applications. *NPG Asia Mater* **2022**;*14*:18.
109. Li Y, Wang J, Qian D, Chen L, Mo X, Wang L, Wang Y, Cui W. Electrospun fibrous sponge via short fiber for mimicking 3D ECM. *J Nanobiotechnol* **2021**;*19*:131.
110. Soliman S, Pagliari S, Rinaldi A, Forte G, Fiaccavento R, Pagliari F, Franzese O, Minieri M, Di Nardo P, Licoccia S, Traversa E. Multiscale three-dimensional scaffolds for soft tissue engineering via multimodal electrospinning. *Acta Biomater* **2010**;*6*:1227.
111. Pham QP, Sharma U, Mikos AG. Electrospun poly(ε-caprolactone) microfiber and multilayer nanofiber/microfiber scaffolds: characterization of scaffolds and measurement of cellular infiltration. *Biomacromol* **2006**;*7*:2796.
112. Han D, Gouma PI. Electrospun bioscaffolds that mimic the topology of extracellular matrix. *Nanomedicine* **2006**;*2*:37.
113. Erisken C, Kalyon DM, Wang H. Functionally graded electrospun polycaprolactone and β-tricalcium phosphate nanocomposites for tissue engineering applications. *Biomaterials* **2008**;*29*:4065.
114. Kim G, Son J, Park S, Kim W. Hybrid process for fabricating 3D hierarchical scaffolds combining rapid prototyping and electrospinning. *Macromol Rapid Comm* **2008**;*29*:1577.
115. Martins A, Chung S, Pedro AJ, Sousa RA, Marques AP, Reis RL, Neves NM. Hierarchical starch-based fibrous scaffold for bone tissue engineering applications. *J Tissue Eng Regen M* **2009**;*3*:37.
116. Moroni L, Schotel R, Hamann D, de Wijn JR, van Blitterswijk CA. 3D fiber-deposited electrospun integrated scaffolds enhance cartilage tissue formation. *Adv Funct Mater* **2008**;*18*:53.
117. Yang XC, Shah JD, Wang HJ. Nanofiber enabled layer-by-layer approach toward three-dimensional tissue formation. *Tissue Eng A* **2009**;*15*:945.
118. Park SH, Kim TG, Kim HC, Yang DY, Park TG. Development of dual scale scaffolds via direct polymer melt deposition and electrospinning for applications in tissue regeneration. *Acta Biomater* **2008**;*4*:1198.
119. Kim SJ, Jang DH, Park WH, Min BM. Fabrication and characterization of 3-dimensional PLGA nanofiber/microfiber composite scaffolds. *Polymer* **2010**;*51*:1320.
120. Zhang X, Cheng X, Si Y, Yu J, Ding B. Elastic and highly fatigue resistant ZrO_2-SiO_2 nanofibrous aerogel with low energy dissipation for thermal insulation. *Chem Eng J* **2022**;*433*:133628.
121. Zhang X, Cheng X, Si Y, Yu J, Ding B. All-ceramic and elastic aerogels with nanofibrous-granular binary synergistic structure for thermal superinsulation. *ACS Nano* **2022**;*16*:5487.
122. Zhang X, Wang F, Dou L, Cheng X, Si Y, Yu J, Ding B. Ultrastrong, superelastic, and lamellar multiarch structured ZrO_2-Al_2O_3 nanofibrous aerogels with high-temperature resistance over 1300 °C. *ACS Nano* **2020**;*14*:15616.
123. Li SZ, Wu F, Zhang X, Han GT, Si Y, Yu JY, Ding B. Flexible Al_2O_3/ZrO_2 nanofibrous membranes for thermal insulation. *CrystEngComm* **1859**;*2022*:24.
124. Zhang X, Liu C, Zhang X, Si Y, Yu J, Ding B. Super strong, shear resistant, and highly elastic lamellar structured ceramic nanofibrous aerogels for thermal insulation. *J Mater Chem A* **2021**;*9*:27415.
125. Wang W, Itoh S, Konno K, Kikkawa T, Ichinose S, Sakai K, Ohkuma T, Watabe K. Effects of Schwann cell alignment along the oriented electrospun chitosan nanofibers on nerve regeneration. *J Biomed Mater Res A* **2009**;*91A*:994.
126. Shim IK, Suh WH, Lee SY, Lee SH, Heo SJ, Lee MC, Lee SJ. Chitosan nano-/microfibrous double-layered membrane with rolled-up three-dimensional structures for chondrocyte cultivation. *J Biomed Mater Res A* **2009**;*90A*:595.
127. Teo WE, Liao S, Chan CK, Ramakrishna S. Remodeling of three-dimensional hierarchically organized nanofibrous assemblies. *Curr Nanosci* **2008**;*4*:361.
128. Ki CS, Kim JW, Hyun JH, Lee KH, Hattori M, Rah DK, Park YH. Electrospun three-dimensional silk fibroin nanofibrous scaffold. *J Appl Polym Sci* **2007**;*106*:3922.
129. Roy S, Kuddannaya S, Das T, Lee HY, Lim J, Hu X, Yoona YC, Kim J. A novel approach for fabricating highly tunable and fluffy bioinspired 3D poly(vinyl alcohol) (PVA) fiber scaffolds. *Nanoscale* **2017**;*9*:7081.

130. Hong S, Kim G. Fabrication of size-controlled three-dimensional structures consisting of electrohydrodynamically produced polycaprolactone micro/nanofibers. *Appl Phys A Mater* **2011**;*103*:1009.
131. Jing X, Li H, Mi HY, Liu YJ, Tan YM. Fabrication of three-dimensional fluffy nanofibrous scaffolds for tissue engineering via electrospinning and CO_2 escaping foaming. *Ind Eng Chem Res* **2019**;*58*:9412.
132. Smit E, Buttner U, Sanderson RD. Continuous yarns from electrospun fibers. *Polymer* **2005**;*46*:2419.
133. Teo WE, Gopal R, Ramaseshan R, Fujihara K, Ramakrishna S. A dynamic liquid support system for continuous electrospun yarn fabrication. *Polymer* **2007**;*48*:3400.
134. Gang EH, Ki CS, Kim JW, Lee J, Cha BG, Lee KH, Park YH. Highly porous three-dimensional poly(lactide-co-glycolide) (PLGA) microfibrous scaffold prepared by electrospinning method: a comparison study with other PLGA type scaffolds on its biological evaluation. *Fiber Polym* **2012**;*13*:685.
135. Yokoyama Y, Hattori S, Yoshikawa C, Yasuda Y, Koyama H, Takato T, Kobayashi H. Novel wet electrospinning system for fabrication of spongiform nanofiber 3-dimensional fabric. *Mater Lett* **2009**;*63*:754.
136. Kasuga T, Obata A, Maeda H, Ota Y, Yao X, Oribe K. Siloxane-poly(lactic acid)-vaterite composites with 3D cotton-like structure. *J Mater Sci Mater Med* **2012**;*23*:2349.
137. Chakrapani VY, Kumar T, Raj DK, Kumary TV. Electrospun 3D composite scaffolds for craniofacial critical size defects. *J Mater Sci* **2017**;*28*:119.
138. Lin YZ, Zhong LB, Dou S, Shao ZD, Liu Q, Zheng YM. Facile synthesis of electrospun carbon nanofiber/graphene oxide composite aerogels for high efficiency oils absorption. *Environ Int* **2019**;*128*:37.
139. Jin L, Wang T, Feng ZQ, Zhu ML, Leach MK, Naim YI, Jiang Q. Fabrication and characterization of a novel fluffy polypyrrole fibrous scaffold designed for 3D cell culture. *J Mater Chem* **2012**;*22*:18321.
140. Yoon CK, Park BK, Lee WI. Characteristics of micro-glass bead/PLA porous composite prepared by electrospinning. *Adv Compos Mater* **2018**;*27*:183.
141. Zhang D, Chang J. Electrospinning of three-dimensional nanofibrous tubes with controllable architectures. *Nano Lett* **2008**;*8*:3283.
142. Park KY, Ramaraj B, Choi WS, Yoon KR. Fabrication and metallization of 3D electrospun nanofiberous architecture with gold and silver coating for applications related to electrochemical supercapacitors. *Mater Chem Phys* **2013**;*142*:600.
143. Chang GQ, Zhu XF, Li AK, Kan WW, Warren R, Zhao RG, Wang XL, Xue G, Shen JY, Lin LW. Formation and self-assembly of 3D nanofibrous networks based on oppositely charged jets. *Mater Design* **2016**;*97*:126.
144. Jin L, Feng ZQ, Wang T, Ren ZZ, Ma SS, Wu JH, Sun DP. A novel fluffy hydroxylapatite fiber scaffold with deep interconnected pores designed for three-dimensional cell culture. *J Mater Chem B* **2014**;*2*:129.
145. Kim TG, Chung HJ, Park TG. Macroporous and nanofibrous hyaluronic acid/collagen hybrid scaffold fabricated by concurrent electrospinning and deposition/leaching of salt particles. *Acta Biomater* **2008**;*4*:1611.
146. Schneider OD, Weber F, Brunner TJ, Loher S, Ehrbar M, Schmidlin PR, Stark WJ. In vivo and in vitro evaluation of flexible, cottonwool-like nanocomposites as bone substitute material for complex defects. *Acta Biomater* **2009**;*5*:1775.
147. Hwang TI, Maharjan B, Tiwari AP, Lee S, Joshi MK, Park CH, Kim CS. Facile fabrication of spongy nanofibrous scaffold for tissue engineering applications. *Mater Lett* **2018**;*219*:119.
148. Lee S, Joshi MK, Tiwari AP, Maharjan B, Kim KS, Yun YH, Park CH, Kim CS. Lactic acid assisted fabrication of bioactive three-dimensional PLLA/β-TCP fibrous scaffold for biomedical application. *Chem Eng J* **2018**;*347*:771.
149. Choi W, Lee S, Kim SH, Jang JH. Polydopamine inter-fiber networks: new strategy for producing rigid, sticky, 3D fluffy electrospun fibrous polycaprolactone sponges. *Macromol Biosci* **2016**;*16*:824.
150. Cheng M, Qin Z, Hu S, Yu H, Zhu M. Use of electrospinning to directly fabricate three-dimensional nanofiber stacks of cellulose acetate under high relative humidity condition. *Cellulose* **2017**;*24*:219.
151. Kim JI, Lee JC, Kim MJ, Park CH, Kim CS. The impact of humidity on the generation and morphology of the 3D cotton-like nanofibrous piezoelectric scaffold via an electrospinning method. *Mater Lett* **2019**;*236*:510.
152. Wu H, Zhao L, Si Y, Zhang S, Yu J, Ding B. Ultralight and superelastic fibrous sponges with effective heat preservation and photo-thermal conversion for personal cold protection. *Compos Commun* **2021**;*25*:100766.
153. Feng Y, Zong D, Hou Y, Yin X, Zhang S, Duan L, Si Y, Jia Y, Ding B. Gradient structured micro/nanofibrous sponges with superior compressibility and stretchability for broadband sound absorption. *J Colloid Interf Sci* **2021**;*593*:59.
154. Xu H, Wang S, Gong X, Yang M, Liu X, Zhang S, Yu J, Ding B. Superelastic, ultralight, and washable electrospun fibrous sponges for effective warmth retention. *Compos Commun* **2022**;*29*:101024.
155. Zong D, Cao L, Li Y, Yin X, Si Y, Yu J, Ding B. Interlocked dual-network and superelastic electrospun fibrous sponges for efficient low-frequency noise absorption. *Small Str* **2020**;*1*:2000004.
156. Zhao L, Wu H, Jiao W, Yin X, Si Y, Yu J, Ding B. Superelastic, lightweight, and flame-retardant 3D fibrous sponge fabricated by one-step electrospinning for heat retention. *Compos Commun* **2021**;*25*:100681.
157. Zhang R, Gong X, Wang S, Tian Y, Liu Y, Zhang S, Yu J, Ding B. Superelastic and fire-retardant nano-/microfibrous sponges for high-efficiency warmth retention. *ACS Appl Mater Interfaces* **2021**;*13*:58027.
158. Zheng Z, Wu H, Si Y, Jia Y, Ding B. Stretchable and resilient fibrous sponges tailored by interlocking double-network for warmth retention. *Compos Commun* **2021**;*27*:100788.
159. Wu H, Li Y, Zhao L, Wang S, Tian Y, Si Y, Yu J, Ding B. Stretchable and superelastic fibrous sponges tailored by "stiff-soft" bicomponent electrospun fibers for warmth retention. *ACS Appl Mater Interfaces* **2020**;*12*:27562.
160. Kalauni K, Pawar SJ. A review on the taxonomy, factors associated with sound absorption and theoretical modeling of porous sound absorbing materials. *J Porous Mat* **2019**;*26*:1795.
161. Tang XN, Yan X. Acoustic energy absorption properties of fibrous materials: a review. *Composites A* **2017**;*101*:360.
162. Wu H, Zhao L, Zhang S, Si Y, Yu J, Ding B. Ultralight and mechanically robust fibrous sponges tailored by semi-interpenetrating polymer networks for warmth retention. *ACS Appl Mater Interfaces* **2021**;*13*:18165.
163. Dou L, Cheng X, Zhang X, Si Y, Yu J, Ding B. Temperature-invariant superelastic, fatigue resistant, and binary-network structured silica nanofibrous aerogels for thermal superinsulation. *J Mater Chem A* **2020**;*8*:7775.
164. Dou L, Si Y, Yu J, Ding B. Semi-template based, biomimetic-architectured, and mechanically robust ceramic nanofibrous aerogels for thermal insulation. *Nano Res* **2022**;*15*:5581.
165. Li Y, Yin X, Yu J, Ding B. Electrospun nanofibers for high-performance air filtration. *Compos Commun* **2019**;*15*:6.
166. Li Y, Cao L, Yin X, Si Y, Yu J, Ding B. Ultrafine, self-crimp, and electret nano-wool for low-resistance and high-efficiency

protective filter media against $PM_{0.3}$. *J. Colloid Interf. Sci.* **2020**;*578*:565.
167. Qian ZC, Wang Z, Chen Y, Tong SR, Ge MF, Zhao N, Xu J. Superelastic and ultralight polyimide aerogels as thermal insulators and particulate air filters. *J Mater Chem A* **2018**;*6*:828.
168. Zhang J, Zhang F, Song J, Liu L, Si Y, Yu J, Ding B. Electrospun flexible nanofibrous membranes for oil/water separation. *J Mater Chem A* **2019**;*7*:20075.
169. Zhang J, Liu L, Si Y, Yu J, Ding B. Electrospun nanofibrous membranes: an effective arsenal for the purification of emulsified oily wastewater. *Adv Funct Mater* **2020**;*30*:2002192.
170. Zhang J, Liu L, Si Y, Yu J, Ding B. Rational design of electrospun nanofibrous materials for oil/water emulsion separation. *Mat Chem Front* **2021**;*5*:97.
171. Lee S, Kim B, Kim SH, Kim E, Jang JH. Superhydrophobic, reversibly elastic, moldable, and electrospun (SupREME) fibers with multimodal functions: from oil absorbents to local drug delivery adjuvants. *Adv Funct Mater* **2017**;*27*:1702310.
172. Fu Q, Liu L, Si Y, Yu J, Ding B. Shapeable, underwater superelastic, and highly phosphorylated nanofibrous aerogels for large-capacity and high-throughput protein separation. *ACS Appl Mater Interfaces* **2019**;*11*:44874.
173. Jang JH, Castano O, Kim HW. Electrospun materials as potential platforms for bone tissue engineering. *Adv Drug Deliver Rev* **2009**;*61*:1065.
174. Dong Y, Zheng Y, Zhang K, Yao Y, Wang L, Li X, Yu J, Ding B. Electrospun nanofibrous materials for wound healing. *Adv Fiber Mater* **2020**;*2*:212.
175. Wang L, Qiu Y, Guo Y, Si Y, Liu L, Cao J, Yu J, Li X, Zhang Q, Ding B. Smart, elastic, and nanofiber-based 3D scaffolds with self-deploying capability for osteoporotic bone regeneration. *Nano Lett* **2019**;*19*:9112.
176. Wang J, Cheng Y, Wang H, Wang Y, Zhang K, Fan C, Wang H, Mo X. Biomimetic and hierarchical nerve conduits from multifunctional nanofibers for guided peripheral nerve regeneration. *Acta Biomater* **2020**;*117*:180.
177. Chen Y, Xu W, Shafiq M, Tang J, Hao J, Xie X, Yuan Z, Xiao X, Liu Y, Mo X. Three-dimensional porous gas-foamed electrospun nanofiber scaffold for cartilage regeneration. *J Colloid Interf Sci* **2021**;*603*:94.

Dingding Zong received her B.S. degree from Henan University of Engineering, China, in 2016. She is now a Ph.D. candidate in Prof. Bin Ding's group. Her current research interests mainly focus on the preparation and application of electrospun fibrous sponges.

Shichao Zhang received his B.S. from Qingdao University, China in 2011. After that, he earned his Ph.D. degree from Donghua University, China, in 2017. Currently, he is a full professor in the Innovation Center for Textile Science and Technology in Donghua University. His research mainly includes electrospun fibrous sponges, filtration materials, oil/water separation materials, etc.

Bin Ding received his B.S. from Northeast Normal University, China, in 1998, and his M.S. from Chonbuk National University, Korea, in 2003. After that, he earned his Ph.D. degree from Keio University, Japan, in 2005. Currently, he is the dean of the institute of science and technology (Donghua university) and has been designated as the "National Science Fund for Distinguished Young Scholar" and the "Changjiang Scholar". His research mainly focuses on electrospun fibrous sponges, flexible ceramic nanofibers, waterproof and breathable materials, filtration materials, oil/water separation materials, etc.